Synthesis, Characterization, and Comparative Theoretical Investigation of Dinitrogen-Bridged Group 6-Gold Heterobimetallic Complexes

David Specklin, Anaïs Coffinet, Laure Vendier, Iker Del rosal, Chiara Dinoi, Antoine Simonneau

Synthesis, characterization and comparative theoretical investigation of dinitrogen-bridged group 6-gold heterobimetallic complexes

David Specklin,[#] Anaïs Coffinet,[#] Laure Vendier,[#] Iker del Rosal,[†] Chiara Dinoi[†] and Antoine Simonneau*[#]*

LCC-CNRS, Université de Toulouse, CNRS, UPS, 205 route de Narbonne, BP44099, F-31077 Toulouse cedex 4, France.

† LPCNO, CNRS & INSA, Université Paul Sabatier, 135 Avenue de Rangueil, 31077 Toulouse, France

ABSTRACT. We have prepared and characterized a series of unprecedented group 6-group 11, N_2-bridged, heterobimetallic $[ML_4(\eta^1\text{-}N_2)(\mu\text{-}\eta^1\text{:}\eta^1\text{-}N_2)Au(NHC)]^+$ complexes (M = Mo, W, L_2 = diphosphine) by treatment of *trans*-$[ML_4(N_2)_2]$ with a cationic gold(I) complex $[Au(NHC)]^+$. The adducts are very labile in solution and in the solid, especially in the case of molybdenum, and decomposition pathways are likely initiated by electron transfers from the zerovalent group 6 atom to gold. Spectroscopic and structural parameters point to the fact that the gold adducts are very similar to Lewis pairs formed out of strong main-group Lewis acids (LA) and low-valent, end-on dinitrogen complexes, with a bent M–N–N–Au motif. To verify how far the analogy goes, we computed the electronic structures of $[W(depe)_2(\eta^1\text{-}N_2)(\mu\text{-}\eta^1\text{:}\eta^1\text{-}N_2)AuNHC]^+$ ($\mathbf{10}_{W^+}$) and

[W(depe)$_2$(η^1-N$_2$)(μ-η^1:η^1-N$_2$)B(C$_6$F$_5$)$_3$] (**11**$_w$). A careful analysis of the frontier orbitals of both compounds shows that a filled orbital resulting from the combination of the π^* orbital of the bridging N$_2$ with a *d* orbital of the group 6 metal overlaps in **10**$_w$ with an empty *sd* hybrid orbital at gold, whereas in **11**$_w$ with a *sp*^{3} hybrid orbital at boron. The bent N–N–LA arrangement maximizes these interactions, providing a similar level of N$_2$ "push-pull" activation in the two compounds. In the gold case, the HOMO-2 orbital is further delocalized to the empty carbenic *p* orbital and an NBO analysis suggests an important electrostatic component in the μ-N$_2$–[Au(NHC)]$^+$ bond.

Introduction

Activation of dinitrogen through its binding to a transition or f-block metal has attracted constant attention from coordination and organometallic chemists for more than 50 years.[1] Beyond the inherent challenge posed by the high stability of the N$_2$ molecule, investigations on dinitrogen activation have been motivated by the quest for sustainable anthropogenic nitrogen fixation methods that could potentially replace the Haber-Bosch process.[2] In this perspective, the nitrogen-fixing enzymes, the nitrogenases,[3] have inspired chemists as they allow dinitrogen reduction to take place under ordinary pressure and temperature thanks to binding and stepwise reduction of N$_2$ at an iron-containing active site. The understanding of the nitrogenases' mechanism has been in continual progression, but the complexity of the enzyme coupled to the difficulty of its study during substrate consumption leaves the whole mechanistic picture partly speculative. Yet, since the advent of the 2000s, many synthetic N$_2$-to-NH$_3$ catalysts based on transition metals (TMs) have been devised.[4] Thanks to in-depth mechanistic investigations made possible by the relative simplicity of the catalytic systems, the design of improved catalysts has recently led to high

turnover numbers.[5] In the vast majority of homogeneous nitrogen fixation systems (including the nitrogenases), the N_2 molecule is proposed to bind an *in situ*-generated low-valent metal complex in an end-on fashion as the first step prior to its protonation. When steric hindrance of the ligand sphere allows it, the diatomic N_2 molecule can bridge two metals with μ-η^1:η^1 hapticity, resulting in homobimetallic complexes. N_2-bridged heterobimetallic complexes of the transition elements are more scarcely encountered among the literature and only a handful have been completely characterized. Generally, the synthesis of μ-η^1:η^1-N_2-bridged heterobimetallic complexes has been aimed at devising original reactivities for the N_2 ligand since in such coordination environment, dinitrogen may be polarized to an extent that is not reached with other coordination modes as a result of "push-pull" activation.[6] Starting from a mononuclear end-on dinitrogen complex, two synthetic approaches can be envisioned to prepare a N_2-bridged heterobimetallic compound and both take advantage of the basicity imparted to the terminal nitrogen atom of the N_2 ligand upon coordination: i) formation of a Lewis acid-base adduct with a Lewis acidic TM complex and ii) halide substitution at a high valent TM complex (Scheme 1). The team of Chatt has systematically investigated the coordination of various early d-block Lewis acids through dative bonding with the terminal N of the N_2 ligand of *trans*-[$ReCl(N_2)(PMe_2Ph)_4$] and recorded more or less important bathochromic shifts of the $\nu(N_2)$ elongation frequency in IR spectroscopy.[7] The enhanced N_2 activation was rationalized according to a push-pull effect and its magnitude was correlated to the electronic configuration of the acceptor metal. Sellmann *et al*. have reported the isolation of [$Cp(CO)_2Mn$–(μ-N_2)–$Cr(CO)_5$] from the reaction of [$CpMn(CO)_2N_2$] with [$Cr(CO)_5(THF)$].[8] Later, the team of Hidai synthesized a series of heterobimetallic N_2-bridged complexes by taking advantage of the nucleophilic nature of the N_2 ligand in Mo^0 and W^0 dinitrogen complexes, which substitutes a chloride ligand in high-valent organometallic compounds of groups 4 and 5.[9] The

group of Seymore has characterized an adduct of the *trans*-[ReCl(N_2)(PMe_2Ph)$_4$] compound with a cationic Mo^{IV} complex while studying heterolytic N_2 splitting.[10] As far as late transition metal acceptors are concerned, stable heterobimetallic complexes were obtained by the formation of Lewis pairs between a low-valent Mo, Re or Fe dinitrogen complex and an electrophilic Fe^{II} complex.[11] All but one[11b,c] of these structurally characterized N_2-bridged complexes show a linear M–N≡N–M' arrangement as a result of *d* orbitals mixing with the π molecular orbitals (MOs) of N_2.

Scheme 1. Syntheses of N_2-bridged heterobimetallic complexes

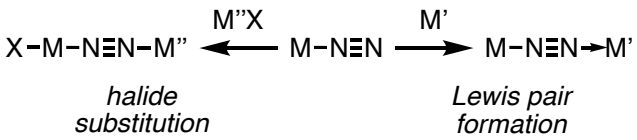

The formation of $B(C_6F_5)_3$ (**1**) adducts with *trans*-[M(dppe)$_2$(N_2)$_2$] [M = Mo, $\mathbf{2}_{Mo}$, M = W, $\mathbf{2}_W$, dppe = 1,2-bis(diphenylphosphino)ethane] and [Fe(depe)$_2$(N_2)] [depe = 1,2-bis(diethylphosphino)ethane] has been reported by us[12] and the team of Szymczak,[11e] respectively. Characterization of these adducts revealed that N_2 activation became significant upon coordination to the strong boron Lewis acid (LA), with a bent N–N–B motif. The Szymczak group rationalized the push-pull effect with the help of DFT calculations, and showed that the boron vacant orbital interacts with a π* one of the N_2 ligand, resulting in a bent structure. Interestingly, these combinations of dinitrogen complexes with main group LA[13] have shown unprecedented reactivities toward N_2 protonation[11e] or functionalization.[12] We now wish to extend this N_2 complex-LA cooperation paradigm and would like to report herein our studies regarding the formation of stable adducts between zero-valent group 6 dinitrogen complexes and cationic gold(I) complexes. With the purpose of exploiting the reactivity of cationic gold(I) compounds toward unsaturated organic molecules[14] for N_2 functionalization (which turned out to be unproductive), we have, as a

interdependent study, examined how Au^{I} and Mo^{0} or W^{0} complexes interact in the condensed phase. We wanted to answer the following questions: are undesirable redox events likely to occur, and if not, would gold coordinate to the N_2 ligand and how? As mentioned above, reactions of early-to-mid LA-TMs with N_2 complexes have been explored thoroughly and mainly resulted in the formation of adducts. By contrast, and to the best of our knowledge, nothing is known with late, beyond group 8 LA–TMs, with the exception of Cu^{II} and Ag^{I} salts, which have been reported to quantitatively oxidize the Re^{I}–N_2 complex *trans*-[$ReCl(N_2)(PMe_2Ph)_4$].[7a] Structural, theoretical and stability data are thus desirable for who wishes to exploit the reactivity of late TMs for the cooperative activation of N_2. Moreover, the isolobal relationship existing between Au^{+} and H^{+}[15] makes the putative adducts relevant models to assess the effect of acidic residues on ligating N_2 within the active site of the nitrogenases and would come to complement the studies carried out by the Szymczak group,[11e,16] whereas the paucity of reports of stable, genuine gold-N_2 complexes in the literature[17] provides further incentive to such investigations. Finally, the above mentioned $B(C_6F_5)_3$-dinitrogen complexes can be well viewed as mixed metal/main group frustrated Lewis pairs (FLPs)[18] activating the N_2 molecule. Replacing boron with gold would introduce an "all-metal" FLP system[19] for N_2 activation.[20,21] In this Article, we wish to report on the synthesis and structural, spectroscopic and electronic characterization of [M–N≡N–Au]$^{+}$ adducts of Au^{I} cations bearing N-heterocyclic carbene ligands (NHC) with group 6 (Mo, W) N_2 complexes.

Experimental Section

Computational Details. Calculations were carried out using the Gaussian 09 package[22] at the DFT level by means of the hybrid density functional B3PW91.[23] Polarized all electron double-zeta 6-31G(d,p) basis set were used for H, C, N, P, B and F atoms. For the W and Au atoms, the Stuttgart-Dresden pseudopotentials were used in combination with their associated basis sets[24]

augmented by a set of polarization functions (f-orbital polarization exponents of 0.823 and 1.05 for the W and Au atoms, respectively).[25] The nature of the optimized stationary point has been verified by means of analytical frequency calculation at 298.15 K and 1 atm. The geometry optimizations have been achieved without any geometrical constraints and include dispersion with the D3 version of Grimme's dispersion with Becke-Johnson damping.[26] Energy data are reported in the gas phase. The electron density and partial charge distribution were examined in terms of localized electron-pair bonding units using the NBO program.[27]

General Considerations. All reactions were performed in flame- or oven-dried glassware with rigorous exclusion of air and moisture, using a nitrogen filled Jacomex glovebox (O_2 < 0.5 ppm, H_2O < 1 ppm). Solvents used were pre-dried (toluene and *n*-pentane by passing through a Puresolv MD 7 solvent purification machine; *n*-hexane and hexamethyldisiloxane (HMDSO) by distillation over CaH_2), degassed by freeze-pump-thaw cycles, dried over molecular sieves and stored in the glovebox. C_6D_6, C_6D_5Cl, and THF-d_8 (purchased from Eurisotop) were degassed by freeze-pump-thaw cycles, dried over molecular sieves and stored in the glovebox. The Mo/W dinitrogen complexes $\mathbf{2}_{Mo}$–$\mathbf{4}_{Mo}$[28], ^{15}N-$\mathbf{3}_{W}$,[28] [Au(NTf$_2$)(Me$_2$Idipp)] (**6b**NTf$_2$)[29] and B(C_6F_5)$_3$ (**1**)[30] were prepared according to reported procedures and stored in the glovebox. The [Au(Cl)(NHC)] complexes **6a–e**Cl, dimethylphenylphosphine (PMe_2Ph), 1,2-bis(diphenylphosphino)ethane (dppe), 1,2-bis(diethylphosphino)ethane (depe), and NaB(C_6H_3-3,5-{CF_3}$_2$)$_4$ were purchased from TCI, Sigma-Aldrich or Strem Chemicals and used as received. ^{1}H, ^{11}B, ^{13}C, ^{19}F and ^{31}P NMR spectra were recorded using NMR tubes equipped with J. Young valves on a Bruker Avance III 400 spectrometer. Chemical shifts are in parts per million (ppm) downfield from tetramethylsilane and are referenced to the most upfield residual solvent resonance as the internal standard (C_6HD_5: δ reported = 7.16 ppm, C_6HD_4Cl: δ reported = 6.96 ppm, THF-d_7: δ reported = 1.72 ppm for ^{1}H NMR; C_6D_5Cl: δ

reported = 125.96 ppm for ^{13}C NMR). ^{11}B, ^{19}F and ^{31}P NMR spectra were calibrated according to the IUPAC recommendation using a unified chemical shift scale based on the proton resonance of tetramethylsilane as primary reference.[31] Data are reported as follows: chemical shift, multiplicity (br = broad, s = singlet, d = doublet, t = triplet, q = quartet, p = quintet, hept = heptuplet, m = multiplet), coupling constant (Hz), and integration. Infrared (IR) spectra were recorded in a nitrogen filled Jacomex glove box (O_2 < 0.5 ppm, H_2O < 1 ppm) on an Agilent Cary 630 FT-IR spectrophotometer equipped with ATR or transmission modules and are reported in wavenumbers (cm^{-1}) with (s) indicating strong absorption. Elemental analyses were performed on samples sealed in tin capsules under Ar or N_2 by the Analytical Service of the Laboratoire de Chimie de Coordination; results are the average of two independent measurements.

Spectroscopic characterization of [W(dppe)$_2$(N_2)(μ-N_2)Au(Idipp)][B(C_6H_3-3,5-{CF_3}$_2$)$_4$] (7a$_w$BAr^F). NMR characterization: C_6D_5Cl (0.5 mL) was added at room temperature to a vial containing [Au(Cl)(Idipp)] (7.4 mg, 12 μmol), NaB(C_6H_3-3,5-{CF_3}$_2$)$_4$ (10.6 mg, 12 μmol, 1 equiv) and [W(dppe)$_2$(N_2)$_2$] (**2**$_w$, 12.4 mg, 12 μmol, 1 equiv). The deep orange suspension was then stirred vigorously for 5 min during which the mixture turned to a dark red solution upon formation of the gold adduct. The mixture was then immediately transferred to an NMR tube equipped with a J. Young valve and analyzed *via* NMR spectroscopy. IR characterization: the same process was conducted with C_6H_5Cl and transferred into an IR transmission cell for measurement of the N_2 ligand region (2400–1600 cm^{-1}).^{1}**H NMR** (400 MHz, C_6D_5Cl): δ 8.27 (br, 8H, *o*-H, C_6H_3-3,5-(CF_3)$_2$), 7.61 (br, 4H, *p*-H, C_6H_3-3,5-(CF_3)$_2$), 7.42 (t, *J* = 7.8 Hz, 2H, *p*-Ar dipp), 7.20 (d, *J* = 7.8 Hz, 4H, *m*-Ar dipp), 7.14–7.04 (m, 8H, Ar dppe), 7.04–6.91 (m, 16H, Ar dppe), 6.87–6.78 (m, 10H, Ar dppe, C*H* imidazole), 6.67 (br, 8H, Ar dppe), 2.38 (hept, *J* = 7.0 Hz, 4H, C*H*(CH_3)$_2$), 2.28 (br, 4H, CH_2CH_2 dppe), 1.98 (br, 4H, CH_2CH_2 dppe), 1.10 (d, *J* = 6.0 Hz, 24H,CH(CH_3)$_2$) ppm. ^{11}**B NMR** (128 MHz,

C_6D_5Cl): δ –6.0 ppm. **^{13}C NMR** (100 MHz, C_6D_5Cl): δ 166.8 (C carbene), 162.5 (q, J_{CF} = 49.9 Hz, *o*-*C*, C_6H_3-3,5-(CF_3)$_2$), 145.6 (C_{Ar} dipp), 136.7 (t, J_{CP} = 9.3 Hz, Ar_{ipso} dppe), 135.3 (br s, *o*-*C*, C_6H_3-3,5-(CF_3)$_2$), 135.0 (t, J_{CP} = 9.1 Hz, Ar_{ipso} dppe), 133.7 (C_{Ar}dipp), 132.8 (t, J_{CP} = 2.7 Hz, *o*-Ar dppe), 132.1 (t, J_{CP} = 2.4 Hz, *o*-Ar dppe), 131.3 (CH_{Ar}dipp), 129.8 (m, *o*-*C*, C_6H_3-3,5-(CF_3)$_2$), 129.4 (s, *p*-Ar dppe), 128.3 (s, *p*-Ar dppe), 128.2 (hidden, *p*-Ar dppe), 125.0 (q, J_{CF} = 272.4 Hz, CF_3), 124.6 (CH_{Ar} dipp), 124.2 (*C*(CH_3) imidazole), 117.8 (br, *p*-*C*, C_6H_3-3,5-(CF_3)$_2$), 31.1–30.5 (m, CH_2CH_2 dppe), 28.9 (*C*H(CH_3)$_2$), 24.6 (CH(*C*H_3)$_2$), 23.6 (CH(*C*H_3)$_2$) ppm. **^{19}F NMR** (376 MHz, C_6D_5Cl): δ –62.0 ppm. **^{31}P NMR** (162 MHz, C_6D_5Cl): δ 45.5 (J_{PW} = 306.1 Hz) ppm. **IR** (C_6H_5Cl, 2400–1600 cm^{-1} range) ν/cm^{-1} = 2085 (N_2), 1851 (μ-N_2).

Spectroscopic characterization of [W(dppe)$_2$(N_2)(μ-N_2)Au(Me_2Idipp)][B(C_6H_3-3,5-{CF_3}$_2$)$_4$] (7b$_w$BAr^F). C_6D_5Cl (0.5 mL) was added at room temperature to a vial containing [Au(Cl)(Me_2Idipp)] (7.8 mg, 12 μmol), NaB(C_6H_3-3,5-{CF_3}$_2$)$_4$ (10.6 mg, 12 μmol) and [W(dppe)$_2$(N_2)$_2$] (**2**$_w$, 12.4 mg, 12 μmol). The deep orange suspension was then stirred vigorously for 5 min during which the mixture turned to a dark purple solution upon formation of the gold adduct. The mixture was then immediately transferred to an NMR tube equipped with a J. Young valve and analyzed *via* NMR spectroscopy. FTIR characterization: the same process was conducted with C_6H_5Cl and transferred into an IR transmission cell for measurement of the N_2 ligand region (2400–1600 cm^{-1}). **^{1}H NMR** (400 MHz, C_6D_5Cl): δ 8.26 (br, 8H, *o*-*H*, C_6H_3-3,5-(CF_3)$_2$), 7.61 (br, 4H, *p*-*H*, C_6H_3-3,5-(CF_3)$_2$), 7.41 (t, *J* = 7.8 Hz, 2H, *p*-Ar dipp), 7.27–7.10 (m, 8H, *m*-Ar dipp, Ar dppe), 7.10–6.91 (m, 20H, Ar dppe), 6.86 (t, *J* = 7.6 Hz, 8H, Ar dppe), 6.62 (br, 8H, Ar dppe), 2.36–2.20 (m, 8H, ^{i}Pr dipp, CH_2CH_2 dppe), 1.96 (br, 4H, CH_2CH_2 dppe), 1.61 (s, 6H, Me imidazole), 1.10 (d, *J* = 6.7 Hz, 12H, ^{i}Pr dipp), 1.07 (d, *J* = 6.8 Hz, 12H, ^{i}Pr dipp) ppm. **^{11}B NMR** (128 MHz, C_6D_5Cl): δ –6.0 ppm. **^{13}C NMR**

(100 MHz, C_6D_5Cl): δ 162.5 (C carbene), 162.5 (q, J_{CF} = 49.6 Hz, *o*-*C*, C_6H_3-3,5-(CF_3)$_2$), 146.0 (C_{Ar} dipp), 137.3 (t, J_{CP} = 9.8 Hz, Ar_{ipso} dppe), 135.3 (br s, *o*-*C*, C_6H_3-3,5-(CF_3)$_2$), 134.9 (t, J_{CP} = 9.8 Hz, Ar_{ipso} dppe), 133.0 (t, J_{CP} = 2.7 Hz, *o*-Ar dppe), 132.1 (C_{Ar}dipp), 132.1 (t, J_{CP} = 2.7 Hz, *o*-Ar dppe), 131.2 (CH_{Ar} dipp), 129.6–129.7 (m, *o*-*C*, C_6H_3-3,5-(CF_3)$_2$), 129.3 (s, *p*-Ar dppe), 128.4–128.2 (hidden, *p*-Ar dppe), 127.6 (*C*(CH_3) imidazole), 124.6 (CH_{Ar} dipp), 125.0 (q, J_{CF} = 272.5 Hz, *C*F_3), 117.8 (br, *p*-*C*, C_6H_3-3,5-(CF_3)$_2$), 31.0 (t, J_{CP} = 10.7 Hz, *C*H_2*C*H_2 dppe), 28.8 (*C*H(CH_3)$_2$), 25.2 (CH(*C*H_3)$_2$), 23.1 (CH(*C*H_3)$_2$), 9.1 (C(*C*H_3) Imidazole) ppm. **^{19}F NMR** (376 MHz, C_6D_5Cl): δ –62.1 ppm. **^{31}P NMR** (162 MHz, C_6D_5Cl): δ 46.2 (J_{PW} = 307.4 Hz) ppm. **IR** (C_6H_5Cl, 2400–1600 cm^{-1} range) ν/cm^{-1} = 2085 (N_2), 1851 (μ-N_2).

General method for the preparation of [W(depe)$_2$(N_2)(μ-N_2)Au(NHC)][B(C_6H_3-3,5-{CF_3}$_2$)$_4$] adducts (10b–e$_w$BAr^F). PhF (1.5 mL) was added at room temperature to a vial containing [Au(Cl)(NHC)] (46 μmol), NaB(C_6H_3-3,5-{CF_3}$_2$)$_4$ (41 mg, 46 μmol) and [W(depe)$_2$(N_2)$_2$] (**3**$_w$, 30 mg, 46 μmol). The red suspension was then stirred vigorously for 5 min during which the mixture turned to a purple (**10b**$_w$BAr^F) or dark red (**10c–e**$_w$BAr^F) solution upon formation of the adducts. The mixture was then poured in precooled pentane (15 mL, –40 °C) and stored overnight at –40 °C to induce the precipitation of purple or dark red mixtures of the adduct and NaCl recovered by decantation. The fine NaCl powder was then stirred up and removed with pentane washes (3 x 5 mL) to recover the complexes as red or purple crystals after brief drying under a N_2 stream.

[W(depe)$_2$(N_2)(μ-N_2)Au(Me_2Idipp)][B(C_6H_3-3,5-{CF_3}$_2$)$_4$] (10b$_w$BAr^F). Recovered as a purple microcrystalline powder (78 mg, R = 80%). **^{1}H NMR** (400 MHz, C_6D_5Cl): δ 8.26 (br, 8H, *o*-*H*, C_6H_3-3,5-(CF_3)$_2$), 7.62 (br, 4H, *p*-*H*, C_6H_3-3,5-(CF_3)$_2$), 7.26 (t, *J* = 7.8 Hz, 2H, *p*-Ar dipp), 7.08 (d, *J*

= 7.8 Hz, 4H, *m*-Ar dipp), 2.27 (hept, *J* = 6.9 Hz, 4H, ^{i}Pr dipp), 1.71–1.47 (m, 16H, PC*H*$_2$CH$_3$), 1.59 (s, 6H, Me imidazole), 1.23–1.05 (m, 8H, CH$_2$CH$_2$ depe), 1.20 (d, *J* = 6.9 Hz, 12H, ^{i}Pr dipp), 1.09 (d, *J* = 6.9 Hz, 12H, ^{i}Pr dipp), 0.89 (m, 12H, PCH$_2$C*H*$_3$), 0.74 (m, 12H, PCH$_2$C*H*$_3$). ^{11}**B NMR** (128 MHz, C$_6$D$_5$Cl): δ –6.1 ppm. ^{19}**F NMR** (376 MHz, C$_6$D$_5$Cl): δ –62.1 ppm. ^{31}**P NMR** (162 MHz, C$_6$D$_5$Cl): δ 34.2 (J_{PW} = 296.2 Hz) ppm. **IR** (C$_6$H$_5$Cl, 2400–1600 cm^{-1} range) ν/cm^{-1} = 2044 (N$_2$), 1796 (μ-N$_2$); (ATR, powder) ν/cm^{-1} = 2960, 2936, 2065(s, N$_2$), 1763(s, μ-N$_2$), 1647, 1610, 1595, 1495, 1461, 1416, 1395, 1353(s), 1279(s), 1218, 1165, 1117(s), 1092, 1060, 1043, 887, 867, 839, 805, 785, 753, 716, 682, 668. **Elem. anal**. calcd. for C$_{81}$H$_{100}$AuBF$_{24}$N$_6$P$_4$W (%): C, 45.69; H, 4.73; N, 3.95. Found: C, 45.46; H, 4.73; N, 3.35.

[W(depe)$_2$(N$_2$)(μ-N$_2$)Au(IMes)][B(C$_6$H$_3$-3,5-{CF$_3$}$_2$)$_4$] (10c$_w$BAr^F). Recovered as a dark red microcrystalline powder (75 mg, R = 85%). ^{1}**H NMR** (400 MHz, C$_6$D$_5$Cl): δ 8.26 (br, 8H, *o-H*, C$_6$H$_3$-3,5-(CF$_3$)$_2$), 7.62 (br, 4H, *p-H*, C$_6$H$_3$-3,5-(CF$_3$)$_2$), 6.81 (s, 4H, Ar Mes), 6.57 (s, 2H, C*H* imidazole), 2.30 (s, 6H, Me Mes), 2.01–1.82 (m, 8H, PC*H*$_2$CH$_3$), 1.87 (s, 12H, Me Mes), 1.80–1.48 (m, 14H, PC*H*$_2$C*H*$_3$, PCH$_2$C*H*$_3$), 1.13–1.05 (m, 8H, CH$_2$CH$_2$ depe), 1.05–0.91 (m, 12H, PCH$_2$C*H*$_3$), 0.81–0.72 (m, 6H, PCH$_2$C*H*$_3$). ^{11}**B NMR** (128 MHz, C$_6$D$_5$Cl): δ –6.0 ppm. ^{19}**F NMR** (376 MHz, C$_6$D$_5$Cl): δ –62.1 ppm. ^{31}**P NMR** (162 MHz, C$_6$D$_5$Cl): δ 32.6 (J_{PW} = 283.8 Hz) ppm. **IR** (C$_6$H$_5$Cl, 2400–1600 cm^{-1} range) ν/cm^{-1} = 2052 (N$_2$), 1767 (μ-N$_2$); (ATR, powder) ν/cm^{-1} = 2969, 2938, 2885, 2057(s, N$_2$), 1741(s, μ-N$_2$), 1610, 1487, 1458, 1416, 1377, 1352(s), 1271(s), 1161, 1118(s), 1029, 980, 931, 885, 868, 852, 839, 804, 744, 715, 682, 668(s). **Elem. anal**. calcd. for C$_{73}$H$_{84}$AuBF$_{24}$N$_6$P$_4$W (%): C, 43.47; H, 4.20; N, 4.17. Found: C, 43.21; H, 4.07; N, 3.21.

[W(depe)$_2$(N$_2$)(μ-N$_2$)Au(^{i}Bu)][B(C$_6$H$_3$-3,5-{CF$_3$}$_2$)$_4$] (10d$_w$BAr^F). Recovered as small dark red crystals (69 mg, R = 81%). ^{1}**H NMR** (400 MHz, C$_6$D$_5$Cl): δ 8.25 (br, 8H, *o-H*, C$_6$H$_3$-3,5-(CF$_3$)$_2$), 7.62

(br, 4H, *p-H*, C_6H_3-3,5-$(CF_3)_2$), 6.64 (s, 2H, C*H* imidazole), 2.54–2.40 (m, 2H, PC$H_2$$CH_3$), 2.17–2.01 (m, 4H, PC$H_2$$CH_3$), 1.96–1.81 (m, 4H, PC$H_2$$CH_3$), 1.73–1.18 (m, 18H, PC$H_2CH_3$, PC$H_2CH_3$), 1.57 (s, 18H, ^{t}Bu), 1.18–1.01 (m, 17H,CH_2CH_2depe, PCH_2CH_3, PCH_2CH_3), 1.00–0.88 (m, 3H,PCH_2CH_3). **^{11}B NMR** (128 MHz, C_6D_5Cl): δ –6.1 ppm. **^{19}F NMR** (376 MHz, C_6D_5Cl): δ –62.1 ppm. **^{31}P NMR** (162 MHz, C_6D_5Cl): δ 34.4 (J_{PW} = 284.6 Hz) ppm. **IR** (C_6H_5Cl, 2400–1600 cm^{-1} range) ν/cm^{-1} = 2050 (N_2), 1775 (μ-N_2); (ATR, powder) ν/cm^{-1} = 2970, 2937, 2881, 2063(s, N_2), 1726(s, μ-N_2), 1609, 1487, 1459, 1409, 1379, 1351(s), 1272(s), 1212, 1158, 1116(s), 1037, 898, 885, 866, 838, 805, 744, 710, 681(s), 667(s). **Elem**. **anal**. calcd. for $C_{63}H_{80}AuBF_{24}N_6P_4W$ (%): C, 39.98; H, 4.26; N, 4.44. Found: C, 39.56; H, 4.19; N, 3.53.

[W(depe)$_2$(N_2)(μ-N_2)Au(IAd)][B(C_6H_3-3,5-{CF_3}$_2$)$_4$] (10e$_w$BAr^F). Recovered as dark brown crystals (78 mg, R = 83%). This method allowed the recovery of crystals fit for X-ray diffraction analysis. **^{1}H NMR** (400 MHz, C_6D_5Cl): δ 8.24 (br, 8H, *o-H*, C_6H_3-3,5-$(CF_3)_2$), 7.61 (br, 4H, *p-H*, C_6H_3-3,5-$(CF_3)_2$), 6.78 (s, 1H, C*H* imidazole), 6.72 (s, 1H, C*H* imidazole), 2.53–2.22 (m, 6H, Ad), 2.17 (s, 8H, Ad), 2.12–1.83 (m, 14H, PC$H_2$$CH_3$,Ad), 1.83–1.66 (m, 8H, PCH_2CH_3, PCH_2CH_3), 1.66–1.45 (m, 14H, Ad, PC$H_2$$CH_3$), 1.43–1.27 (m, 6H, PC$H_2CH_3$), 1.15–0.88 (m, 22H,PC$H_2CH_3$, CH_2CH_2 depe, Ad). **^{11}B NMR** (128 MHz, C_6D_5Cl): δ –6.1 ppm. **^{19}F NMR** (376 MHz, C_6D_5Cl): δ –62.1 ppm. **^{31}P NMR** (162 MHz, C_6D_5Cl): δ 34.6 (J_{PW} = 295.3 Hz) ppm. **IR** (C_6H_5Cl, 2400–1600 cm^{-1} range) ν/cm^{-1} = 2048 (N_2), 1783 (μ-N_2); **IR** (ATR, powder) ν/cm^{-1} = 2915, 2859, 2048 (N_2), 1762(s, μ-N_2), 1610, 1457, 1353(s), 1274(s), 1160, 1122(s), 1038, 1027, 899, 887, 867, 839, 807, 744, 724, 716, 693, 682(s), 669(s). **Elem**. **anal**. calcd. for $C_{75}H_{92}AuBF_{24}N_6P_4W$ (%): C, 43.96; H, 4.53; N, 4.10. Found: C, 43.40; H, 4.63; N, 3.17. **[W(depe)$_2$($^{15}N_2$)(μ-$^{15}N_2$)Au(IAd)][B(C_6H_3-3,5-{CF_3}$_2$)$_4$] (^{15}N-10e$_w$BAr^F).** **^{15}N NMR** (60 MHz, C_6D_5Cl): δ –40.1 (s, 1N, μ-$N_α$), –42.9 (s, 1N, $N_β$), –

76.1 (s, 1N, N_α), –119.0 (s, 1N, μ-N_β) ppm. **$^{31}P\{^1H\}/^{183}W$ HMQC-NMR** (25 MHz, C_6D_5Cl): δ –2031.1 ppm. **IR** (ATR, powder) ν/cm^{-1} = 2914, 1977 (N_2), 1703(s, μ-N_2), 1458, 1352(s), 1303, 1274(s), 1197, 1161, 1122(s), 1104, 1038, 1027, 930, 899, 887, 866, 838, 807, 755, 743, 724, 715, 710, 693, 681(s), 668(s), 607.

Preparation of [Mo(depe)$_2$(N_2)(μ-N_2)B(C_6F_5)$_3$)] (11$_{Mo}$). Toluene (0.6 mL) was added to a 10-mL flask containing *trans*-[Mo(depe)$_2$(N_2)$_2$] (**3**$_{Mo}$, 34 mg, 60 μmol, 1.0 equiv) and B(C_6F_5)$_3$ (**1**, 31 mg, 60 μmol, 1.0 equiv). After stirring for 10 min at room temperature the orange-brown mixture was filtered, layered slowly with pentane (6 mL) and stored at –40 °C. After two days, orange crystals of **11**$_{Mo}$ were recovered and dried under vacuum (34 mg, 53% yield). Single crystals suitable for X-ray diffraction analysis were obtained from the same crop. **^1H NMR** (400 MHz, C_6D_6): δ 1.76–1.28 (m, 17H), 1.17 (m, 6H), 1.03–0.83 (m, 13H), 0.83–0.69 (m, 10H), 0.67–0.55 (m, 1H), 0.53–0.41 (m, 1H) ppm. **^{11}B NMR** (128 MHz, C_6D_6): δ –10.1 ppm. **^{19}F NMR** (376.5 MHz, C_6D_6): maj (84%): δ –131.9 (d, *J* = 21.6 Hz, 2F), –158.7 (t, *J* = 20.4 Hz, 1F), –164.4 (t, *J* = 18.2 Hz, 2F) ppm; min (16%): δ –132.3 (d, *J* = 19.5 Hz, 2F), –159.5 (t, *J* = 20.7 Hz, 1F), –165.0 (t, *J* = 19.1 Hz, 2F) ppm. **$^{31}P\{^1H\}$ NMR** (162 MHz, C_6D_6): δ 53.0 ppm. **IR** (ATR) ν/cm^{-1} = 2965, 2939, 2909, 2881, 2120 (N_2), 1789 (μ-N_2), 1642, 1512, 1461, 1379, 1279, 1081, 1028, 973, 867, 802, 748, 735, 674, 666, 603, 522. **Elem. anal**. calcd. for $C_{38}H_{48}BF_{15}MoN_4P_4$ (%): C, 42.40; H, 4.49; N, 5.20. Found: C, 42.60; H, 4.25; N, 4.47.

Preparation of [W(depe)$_2$(N_2)(μ-N_2)B(C_6F_5)$_3$)] (11$_W$). Toluene (1.5 mL) was added to a 10-mL flask containing *trans*-[W(depe)$_2$(N_2)$_2$] (**3**$_W$, 65 mg, 100 μmol, 1.0 equiv) and B(C_6F_5)$_3$ (**1**, 51 mg, 100 μmol, 1.0 equiv). After stirring for 10 min at room temperature the orange-brown mixture was filtered, layered slowly with pentane (10 mL) and stored at –40 °C. After one week, purple crystals

of **11**$_W$ were recovered and dried under vacuum (72 mg, 62% yield). Single crystals suitable for X-ray diffraction analysis were obtained from the same crop. ^{1}**H NMR** (400 MHz, Toluene-d_8): δ 1.67–1.28 (m, 20H), 1.22–1.08 (br, 4H), 0.94–0.84 (m, 12H), 0.84–0.70 (m, 12H) ppm. ^{11}**B NMR** (128 MHz, C_6D_6): δ –11.1 ppm.^{19}**F NMR** (377 MHz, Toluene-d_8): δ –132.0 (d, J = 23.8 Hz, 6F), –159.1 (t, J = 20.7 Hz, 3F), –164.6 (td, J = 22.8, 7.4 Hz, 6F) ppm. ^{31}**P{^{1}H} NMR** (162 MHz, C_6D_6): δ 34.7 (J_{PW} = 294 Hz) ppm.**IR** (ATR) ν/cm^{-1} = 2967, 2934, 2910, 2076 (N_2), 1767 (μ-N_2), 1641, 1512, 1461, 1378, 1279, 1081, 1028, 973, 868, 802, 749, 693, 675, 612, 525. **Elem**. **anal**. calcd. for $C_{38}H_{48}BF_{15}WN_4P_4$ (%): C, 39.20; H, 4.16; N, 4.81. Found: C, 39.59; H, 4.09; N, 4.08. **[W(depe)$_2$(^{15}N$_2$)(μ-^{15}N$_2$)B(C$_6$F$_5$)$_3$)]** (**^{15}N-11$_W$**). The preparation is identical than for **11**$_W$. ^{15}**N NMR** (60 MHz, C_6D_6): δ –37.4 (s, 1N, N_β), –55.0 (s, 1N, μ-N_α), –73.9 (s, 1N, N_α), –152.6 (s, 1N, μ-N_β) ppm. ^{31}**P{^{1}H}/^{183}W HMQC-NMR** (25 MHz, C_6D_6): δ –1914.2 ppm. **IR** (ATR) ν/cm^{-1} = 2007 (N_2), 1767 (μ-N_2), 1641, 1512, 1461, 1378, 1279, 1081, 1028, 973, 867, 801, 748, 693, 675, 612.

Results and Discussion

Coordination of Au(I) cations to dinitrogen complexes. Our study commenced by investigating the formation of heterobimetallic [M–N≡N–Au]$^+$ adducts between the group 6 (Mo, W) dinitrogen complexes [M(dppe)$_2$(N_2)$_2$] (**2**$_M$), [M(depe)$_2$(N_2)$_2$] (**3**$_M$), and [M(PMe_2Ph)$_4$ (N_2)$_2$] (**4**$_M$), and Au(I) cations supported by NHC ligands. Due to their strong σ-donor character and their steric profiles, NHCs are well known to provide both excellent stabilization of Au(I) complexes and enhancement of their catalytic activities.[32] Independently of the ligand, monoligated cationic Au(I) complexes are notoriously unstable and tend to readily decompose to colloidal gold, precluding their isolations.[33] Thus, we elected to assess two strategies: i) reaction of the N_2 complexes on [Au(Cl)(NHC)] to form μ-N_2 heterobimetallic complexes by displacement of the chloride ligand

or ii) generation of monoligated Au(I) cations *in situ* in the presence of the N_2 complexes (Scheme 2). Considering that H^+ and Au^+ are isolobal, the first approach could be regarded as analogous to reactions of group 6 N_2 complexes with HCl, which are known to afford the protonated products $[M(Cl)(NNH_2)(L)_4]Cl$.[34] The second strategy requires the generation of the Au(I) cation. The standard approach to prepare $[Au(NHC)]^+$ is through the treatment of [Au(Cl)(NHC)] complexes with the corresponding Ag^+ salt to form AgCl. However, the exact nature of $[Au(NHC)]^+$ complexes in the presence of Ag^+ has recently been questioned in view of Ag^+ effect on catalytic activity and NMR analytic data of some Au(I) complexes.[35] Moreover, the redox potential of Ag/AgCl (0.22 V *vs* SHE) lies above the redox potentials of the dinitrogen complexes considered ($\mathbf{2}_M \approx 0.09$ V, $\mathbf{3}_M \approx$ –0.2 V *vs* SHE)[36] and adventitious remains of Ag^I could lead to undesired redox reactions that would compromise the analysis of the reaction's outcome. A more suitable strategy is to form Au(I) cations by salt metathesis between a sodium salt of an adequate counteranion and Au(Cl)(NHC) complexes. To avoid competition between the anion and dinitrogen for coordination to the gold center we used the noncoordinating anion tetrakis(3,5-bis(trifluoromethyl)phenyl) borate ($[BAr^F]^-$). Cationic gold complexes with anions showing low gold affinity such as BAr^F have been observed in some cases to have increased catalytic efficiency and equal robustness than salts of more coordinating anions.[35,37]

Scheme 2. Synthetic strategies to probe the formation of [M–N≡N–Au] heterobimetallic complexes.

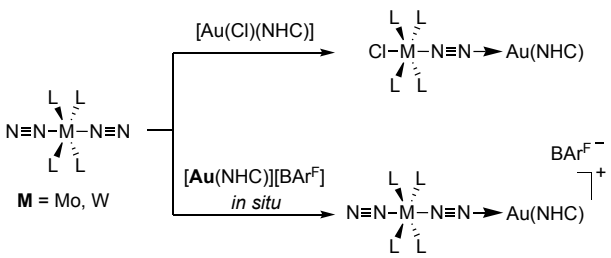

Reaction of [Au(Cl)(NHC)] with $\mathbf{2}_w$. In tetrahydrofuran-d_8 (THF-d_8), $\mathbf{2}_w$ was reacted with 1 equiv of [Au(Cl)(Idipp)] (see SI for details; Idipp: 1,3-bis(2,6-diisopropylphenyl)imidazolin-2-ylidene). Over 18 h at 75 °C, the ^{1}H NMR signature of $\mathbf{2}_w$ slowly disappeared concomitantly with the formation of a well-defined new set of signals for the Idipp moiety and clear markers of the buildup of paramagnetic species such as numerous broad signals in ^{1}H NMR and loss of signals in ^{31}P NMR. X-ray diffraction study on dark red crystals that precipitated out of the solution allowed to characterize the W(I), Au(I) salt $[W(Cl)_2(dppe)_2][Au(Idipp)_2]$ ($\mathbf{5}_w$) as one of the products of the reaction (isolated in 32% yield relative to W content) (Figure 1). Further heating of the reaction mixture led to the deposition of the W(II) complex $[W(Cl)_2(dppe)_2]$ as bright red crystals (up to 18% yield relative to W content after three days at 75 °C).

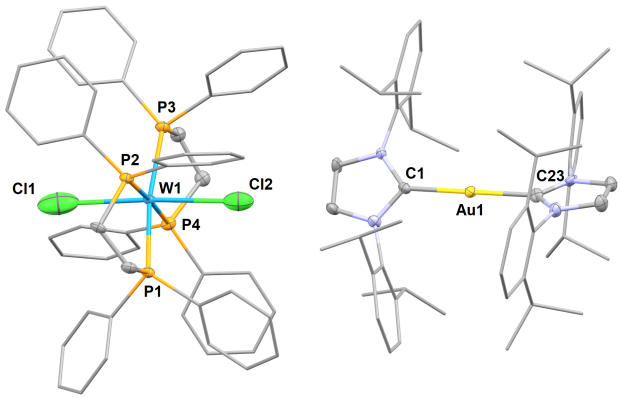

Figure 1. Molecular structure of complex $\mathbf{5}_w$ in the solid state (ellipsoids are drawn at the 50% probability level, ligand substituents are drawn with wireframe and hydrogen atoms are omitted for clarity). Selected bond lengths (Å) and angles (°): C1–Au1 2.033(4), C23–Au1 2.026(4), Cl1–W1 2.732(3), Cl2–W1 2.6674(19), P1–W1 2.4108(11), P2–W1 2.4188(11), P3–W1 2.4308(11), P4–W1 2.4408(11), C1–Au1–C23 179.36(18), Cl1–W–Cl2 176.41.

The $[W(Cl_2)_2(dppe)_2]^-$ anion of $\mathbf{5}_W$ lies in a slightly distorted octahedral geometry with two chloride ligands in *trans* relationship. The formal +I oxidation state of the tungsten is inferred from charge balance and from the dimension of the WCl_2P_4 core, which follows the tendency established between the isostructural neutral complex of W(II) and the cationic complex of W(III) (shorter W–P distances and longer W–Cl distances for decreasing oxidation states).[38] The structural parameters of the cation are comparable to those reported for $[Au(Idipp)_2][BF_4]$.[39] The gold(I) center bears two Idipp ligands in a linear geometry, arranged with a 47.95 ° torsion angle between the imidazolyl planes to minimize the steric repulsion between the carbene fragments. Evidently, two equivalents of [Au(Cl)(Idipp)] are necessary for the formation of $\mathbf{5}_W$ and $[W(Cl)_2(dppe)_2]$, the former producing a Au(0) species that has not been identified. However, reacting $\mathbf{2}_W$ with 2 equiv of [Au(Cl)(Idipp)] does not increase the yield of these complexes significantly, indicating that there are multiple pathways to the formation of paramagnetic species and decomposition of the Au(I) cation. No reaction takes place at room temperature or in less coordinating solvent (in the latter case owing to the poor solubility of [Au(Cl)(Idipp)]). Thus, even if a reactivity similar to HCl could take place to form complexes such as $[W(Cl)(dppe)_2(\mu\text{-}N_2)(Au(Idipp)]$, the harsh conditions necessary to form them favors *in fine* electronic transfer reactions.

Generation of monoligated Au(I) cation *in situ*. We then investigated a series of $[Au(NHC)]^+$ cations ($\mathbf{6}^+$) (Scheme 3) for their coordination to N_2 complexes $\mathbf{2}_M$, $\mathbf{3}_M$, and $[M(PMe_2Ph)_4(N_2)_2]$ [M = Mo, $\mathbf{4}_{Mo}$,(80:20 cis/trans mixture); M = W, $\mathbf{4}_W$ (only cis)].

Scheme 3. Group 6 dinitrogen complexes surveyed (top, M = Mo or W) and formation of [Au(NHC)][BAr^F] salts and selection of the NHCs used in this work (bottom).

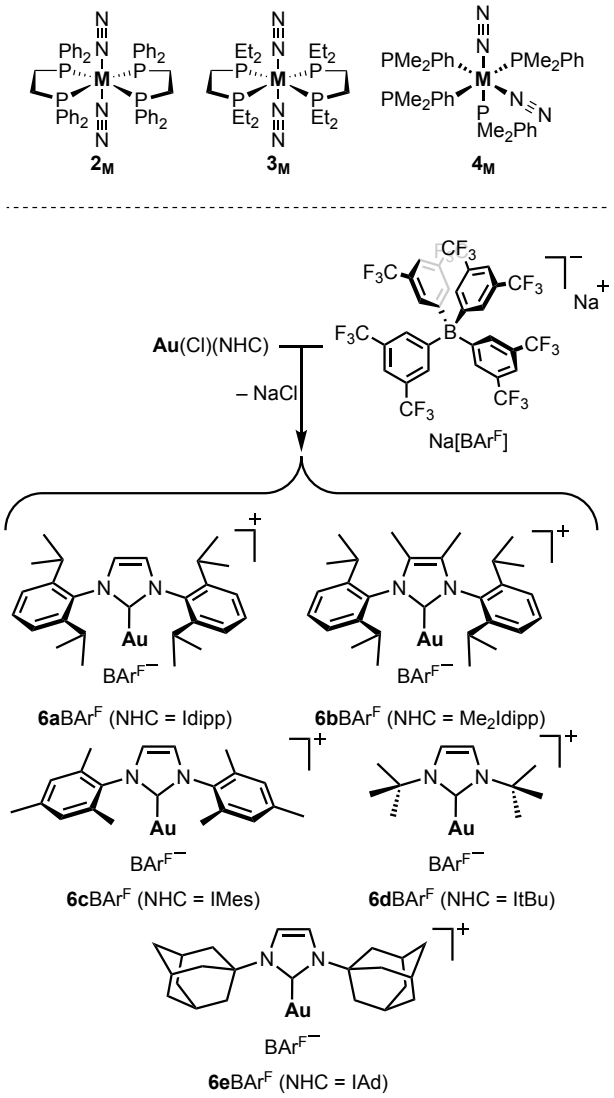

We first explored the reaction of the *in situ* generated [(Idipp)Au][BAr^F] (**6a**BAr^F) with 1 equiv of *trans*-[$Mo(N_2)_2(dppe)_2$] $\mathbf{2}_{Mo}$ at room temperature in chlorobenzene-d_5. Within a few minutes, a mixture of several compounds formed according to NMR spectroscopy. During the first hour of the reaction the major product (≈ 60%) was presumed to be the heterobimetallic adduct *trans*-[$Mo(N_2)(dppe)_2(\mu\text{-}N_2)Au(Idipp)$][$BAr^F$] $\mathbf{7a}_{Mo}BAr^F$. This complex was identified by a singlet in $^{31}P\{^1H\}$ NMR at δ = 63.5 ppm, shifted upfield compared to $\mathbf{2}_{Mo}$ (δ = 65.7 ppm), and by two bands in IR spectroscopy at 1865 and 2127 cm^{-1} assignable to the elongated bridging Mo–N_2–Au moiety and the N_2 in trans position, respectively (*vs*. 1974 cm^{-1} for $\mathbf{2}_{Mo}$). The mixture evolved rapidly, since

after 3 h at RT **7a**$_{Mo}$BAr^F only amounted to ≈ 20% of the mixture and had disappeared after 18 h. Decomposition of **7a**$_{Mo}$BAr^F occurred predominantly through the abstraction of a phosphine ligand by **6a**$^+$ to yield the new complex [(dppe)Mo(μ-η^1:η^1:η^6-dppe)Au(Idipp)][BAr^F] **8**$_{Mo}$ (≈ 80%; Figure 2). Bright red single crystals fit for X-ray diffraction analysis of **8**$_{Mo}$ could be recovered among polycrystalline materials upon slow diffusion of pentane into the crude mixture; however, efforts to isolate or recover single crystals of **7a**$_{Mo}$BAr^F were unsuccessful.

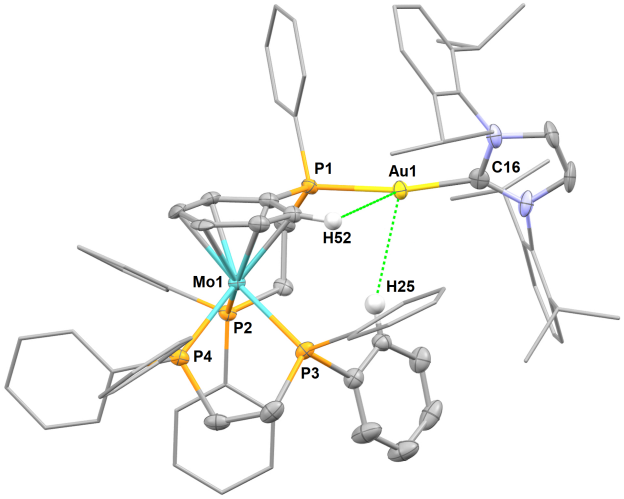

Figure 2. Molecular structure of complex **8**$_{Mo}$ in the solid state (ellipsoids are drawn at the 50% probability level, some ligand substituents are drawn with wireframe, all hydrogen atoms not interacting with the gold center and the BAr^F anion are omitted for clarity). Selected distances (Å) and angles (°): Mo1–P2 2.471(2), Mo1–P3 2.444(2), Mo1–P4 2.446(2), Au1–P1 2.283(2), Au1–C16 2.034(7), Au1–H25 2.881, Au1–H52 2.878, P1–Au1–C16 169.5(2).

The Mo center adopts a three-legged piano stool geometry with a dppe unit coordinated classically with two phosphorus atoms and the other dppe unit chelating through one phosphorus atom and a phenyl substituent of the other phosphorus atom in an η^6 coordination mode. The second phosphorus is coordinated to the gold center of **6a**, which lies in a distorted linear geometry

(169.5 °) to accommodate for agostic interactions with hydrogen atoms of the Mo coordinated phenyl ring and a second phenyl substituent. NMR analysis of the mixture containing $\mathbf{8}_{Mo}$ is coherent with the conservation of this structure in solution. The ^{1}H NMR spectrum shows a set of five protons at δ = 3.26, 3.49, 3.73, 4.58, and 4.63 ppm diagnostic of a η^{6}-phenyl on the Mo center, in line with the chemical shifts of η^{6}-phenylphosphine ligands found on comparable Mo complexes.[40] The agostic interaction between the gold center and the two *ortho* protons of one phenyl substituent is corroborated by a particularly upfield signal at 5.46 ppm in ^{1}H NMR. All phosphine ligands are inequivalent: in $^{31}P\{^{1}H\}$ NMR three resonances show coupling to each other at δ = 76.6, 75.1 and 41.9 ppm, the fourth signal for the phosphine coordinated to the gold cation being found at δ = 26.7 ppm.

Attempts to produce crystals of $\mathbf{7a}_{Mo}BAr^{F}$ and $\mathbf{8}_{Mo}$ led in some occasions to the formation of minute amounts of dark yellow crystals identified by X-ray diffraction analysis as $[Mo(Cl)(N_2)(dppe)_2]$ ($\mathbf{9}_{Mo}$, Figure 3). The Mo^{I} center in $\mathbf{9}_{Mo}$ is stabilized by a chloride ligand presumably sourced from the NaCl formed by salt metathesis between $NaBAr^{F}$ and [Au(Cl)(Idipp)]. $\mathbf{9}_{Mo}$ has an octahedral geometry with dinitrogen and chloride ligands in a *trans* position, both statistically disordered within the crystal lattice.[41] The formation of Mo^{I} species can reasonably be attributed to electronic transfers between Mo^{0} and Au^{I} even though the nature of the accompanying Au^{0} species has not been determined.

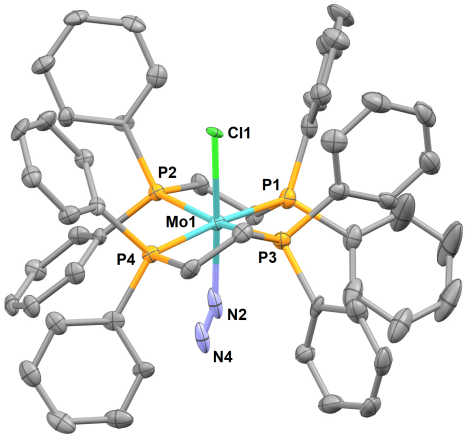

Figure 3. Molecular structure of complex $\mathbf{9}_{Mo}$ in the solid state (ellipsoids are drawn at the 50% probability level, hydrogen atoms are omitted for clarity). Selected bond lengths (Å) and angles (°): Mo1–Cl1 2.396(7), Mo1–N2 2.15(5), P1–Mo1 2.4796(19), P2–Mo1 2.5083(18), P3–Mo1 2.4622(19), P4–Mo1 2.5032(18), Cl1–W–N2 177.1(12).

Reaction of *trans*-[$W(N_2)_2(dppe)_2$] ($\mathbf{2}_w$) with **6a**BAr^F and [$Au(Me_2Idipp)$][BAr^F] (**6b**BAr^F, Me_2Idipp: 1,3-bis[2,6-bis(1-methylethyl)phenyl]-1,3-dihydro-4,5-dimethyl-2H-imidazol-2-ylidene) produced very similar results, which is unsurprising given the structural closeness between the two NHC ligands. $\mathbf{2}_w$ was reacted with 1 equiv of **6a**BAr^F or **6b**BAr^F at room temperature in chlorobenzene-d_5. Analyses of the reaction mixtures by NMR and IR spectroscopies were indicative of the immediate formation of the heterobimetallic adducts [$W(N_2)(dppe)_2(\mu$-$N_2)Au(Idipp)$][BAr^F] ($\mathbf{7a}_w BAr^F$) and [$W(N_2)(dppe)_2(\mu$-$N_2)Au(Me_2Idipp)$][BAr^F] ($\mathbf{7b}_w BAr^F$) (Scheme 4). The $^{31}P\{^1H\}$ NMR spectra of the adducts display a single peak shifted upfield compared to $\mathbf{2}_w$ (δ = 46.2 ppm) at 45.5 ppm (J_{PW} = 320.3 Hz, $\mathbf{7a}_w BAr^F$) or 46.2 ppm (J_{PW} = 307.4 Hz, $\mathbf{7b}_w BAr^F$). The ^1H NMR spectrum showed two inequivalent sets of methylene protons indicating a decreased symmetry at the W center. There is a single set of signals for the NHCs, and $\mathbf{7a}_w BAr^F$ presents a slight downfield shift for the protons of the backbone of the imidazole fragment. This was

attributed to a decrease of electronic density due to the delocalization of the π-electrons toward the more acidic gold center. This increased acidity is also corroborated by the significant upfield shift of the carbenic carbons in ^{13}C NMR at 166.6 ppm (**7a**$_w$BAr^F) and 162.5 ppm (**7b**$_w$BAr^F) vs 176.8 and 172.8 ppm for the corresponding [Au(Cl)(NHC)] complexes. The ^{13}C NMR carbenic carbon chemical shift of **7a**$_w$BAr^F is comparable to that of isolated acetonitrile adducts of [Au(NCMe)(Idipp)]$^+$ salts.[42] The spectral signatures in ^{11}B and ^{19}F NMR are typical of the BAr^F anion.

Scheme 4. Synthesis and proposed identity of 7a$_w$BAr^F and 7b$_w$BAr^F.

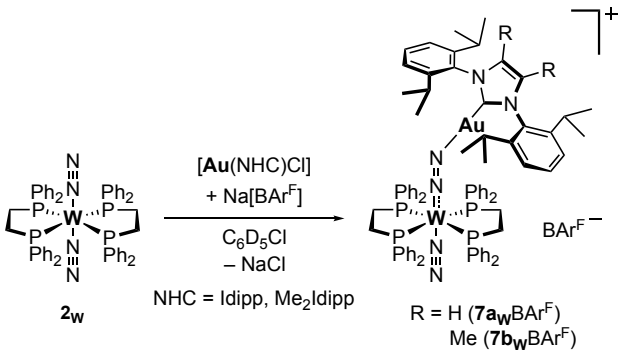

Adducts **7a**$_w$BAr^F and **7b**$_w$BAr^F retain both N_2 ligands in solution according to infrared measurements in chlorobenzene that showed two broad, intense bands at 1851 and 2085 cm^{-1} assignable to the elongated bridging W–N_2–Au moiety and the mono ligated N_2, respectively (*vs*. 1947 cm^{-1} for **2**$_w$ in PhCl). The shift to higher wavenumbers in the IR spectra (*vs*. **2**$_w$) of the N_2 in trans position is diagnostic of decreased N_2 activation. Accordingly, **7a**$_w$BAr^F and **7b**$_w$BAr^F are unreactive toward a second equivalent of [Au(NHC)]$^+$. After *in situ* formation in chlorobenzene-d_5, the adducts are stable for hours but **2**$_w$ is slowly recovered over a period of days. Attempts to remove the solvent under vacuum or to precipitate **7a**$_w$BAr^F and **7b**$_w$BAr^F by treatment of the solution with pentane or hexamethyldisiloxane yielded predominantly **2**$_w$ (> 50%) as well as multiple uncharacterized W complexes and several sets of signals for the NHC moieties are

observed in ^{1}H NMR. The instability of **7a**$_{W}$BAr^{F} and **7b**$_{W}$BAr^{F} generated in this manner precluded their isolation and characterization by X-ray diffraction techniques. Recovery of **2**$_{Mo}$/**2**$_{W}$ from adducts **7a**$_{W}$BAr^{F} and **7b**$_{W}$BAr^{F} suggests that the free gold cations are in equilibrium with the gold cations coordinated to the N_2 complex. The inherent instability of monoligated gold cations in solution might then result in their decomposition. These equilibria are evidenced by the presence of a small band corresponding to the N_2 ligands of **2**$_{Mo}$/**2**$_{W}$ in the infrared measurement of the adducts in chlorobenzene (1947 cm^{-1} for **2**$_{W}$). There is no interaction between **2**$_{W}$ and **6a**$^{+}$ in THF-d_8, the latter forming the THF adduct [Au(THF)(Idipp)]$^{+}$ already reported in the literature.[42] The weak gold coordination to N_2 in **7a**$_{W}$BAr^{F} and **7b**$_{W}$BAr^{F} could stem from the steric bulk of both the gold NHCs and the N_2 complexes' phosphine ligands.

We then explored the formation of adducts with [Au(IMes)]$^{+}$ (**6c**$^{+}$, IMes: 1,3-bis(2,4,6-trimethylphenyl)imidazol-2-ylidene) and [Au(I^{t}Bu)]$^{+}$ (**6d**$^{+}$, I^{t}Bu: 1,3-di-tert-butylimidazol-2-ylidene) that present a reduced steric hindrance at the gold center (*vs*. **6a**$^{+}$ and **6b**$^{+}$). **2**$_{Mo}$ reacted with **6c**BAr^{F} or **6d**BAr^{F} in chlorobenzene-d_5 at RT to yield complex mixtures upon solvation of the gold cations. The main products visible within the first hour (> 60% in both cases) showed spectroscopic signatures similar to **8**$_{Mo}$, diagnostic of η^6-phenyl coordination to the Mo center with a set of five broad signals in ^{1}H NMR (Figures S67 and S69). Phosphine coordination to the gold centers are characterized by signals in ^{31}P{^{1}H} NMR at δ = 29.8 and 29.3 ppm for **6c**$^{+}$ and **6d**$^{+}$ respectively. The lower steric hindrance at the gold center seemingly favors abstraction of the phosphine ligand as no putative N_2 adduct could be observed contrary to reaction of **2**$_{Mo}$ with **6a**BAr^{F}. The reaction of **2**$_{W}$ with one equiv. of **6c**BAr^{F} or **6d**BAr^{F} in chlorobenzene-d_5 at RT allowed immediate observation of the putative adducts [W(N_2)(dppe)$_2$(μ-N_2)Au(NHC)][BAr^{F}] characterized by singlets in ^{31}P{^{1}H} NMR at δ = 44.4 and 45.8 ppm for **7c**$_{W}$BAr^{F} and **7d**$_{W}$BAr^{F}, respectively, that

are upfield-shifted compared to $\mathbf{2}_{W}$ (δ = 46.2 ppm). Infrared analysis of aliquots taken immediately after the mixing of $\mathbf{2}_{W}$ and **6c**BAr^{F} (or **6d**BAr^{F}) in chlorobenzene also supports adduct formation with the presence of two vibrations at 1865 cm^{-1} (**7d**$_{W}BAr^{F}$: 1855 cm^{-1}) and 2077 cm^{-1} (**7d**$_{W}BAr^{F}$: 2077 cm^{-1}) corresponding to the bridging W–N_2–Au moiety and the N_2 in trans relationship, respectively (*vs*. 1947 cm^{-1} for $\mathbf{2}_{W}$ in PhCl). These adducts are short lived, as they represented approximatively 60% of the mixture after 30 min at room temperature and had completely decomposed after 4 h to yield an intractable mixture of paramagnetic compounds and complexes issued from phosphine abstractions. Due to their instability, these putative adducts could not be further characterized or isolated. As $\mathbf{2}_{W}$ is not recovered, their decomposition process stands in contrast with the decomposition of **7a**$_{W}BAr^{F}$ and **7b**$_{W}BAr^{F}$. This can be rationalized by a stronger gold coordination to the dinitrogen ligand owing to the reduced steric strain, which is however balanced by an increased aptitude to engage in phosphine abstraction reaction (presumably driven by steric relief at the W center). The formation of paramagnetic complexes as testified by broad signals in ^{1}H NMR could also be favored by the reduced steric congestion, offering easier pathways for electronic transfers to take place (*vs*. **7a**$_{W}BAr^{F}$ and **7b**$_{W}BAr^{F}$).

To assess the influence of the steric congestion of the N_2 complex, we explored the coordination of **6a**$^{+}$ to complexes [$M(PMe_2Ph)_4(N_2)_2$] ($\mathbf{4}_{M}$), which offer reduced steric hindrance and increased flexibility of the ligand spheres compared to the dppe complexes. We reacted a cis/trans mixture of [$Mo(N_2)_2(PMe_2Ph)_4$] ($\mathbf{4}_{Mo}$) with one equiv. of **6a**BAr^{F} in chlorobenzene-d_5 at room temperature and we observed that the orange solution rapidly turned dark red upon solvation of the gold salt. The heteroleptic complex [Au(Idipp)(PMe_2Ph)][BAr^{F}] was obtained quantitatively within minutes, characterized by a signal at δ = 11.5 ppm in $^{31}P\{^{1}H\}$ NMR spectroscopy (Scheme 5) and identified by its isolation from the reaction mixture (see SI). Under the same conditions as with *cis*-

$[Mo(N_2)_2(PMe_2Ph)_4]$ ($\mathbf{4}_{Mo}$), the phosphine abstraction on *cis*-$[W(N_2)_2(PMe_2Ph)_4]$ ($\mathbf{4}_{W}$) by **6a**$^+$ proceeded at a much slower rate, allowing for **6a**$^+$ to engage in electron transfer reactions with the thus-formed unsaturated W complex, producing uncharacterized paramagnetic compounds.

Scheme 5. Phosphine abstraction on $\mathbf{4}_{Mo}$ to form [Au(Idipp)(PMe$_2$Ph)][BAr^F].

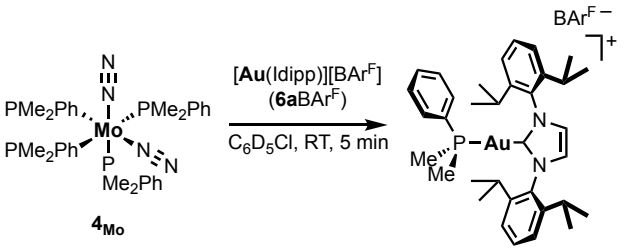

The facile abstraction of the monodentate phosphine highlighted the need to use chelating phosphine ligands able to limit phosphine abstraction while presenting a reduced steric profile compared to dppe. To this end, we then explored the coordination of gold cations to $\mathbf{3}_{W}$. The depe ligand presents the double advantage of being less encumbered and more electron donating than dppe. The reduced steric bulk should allow for a closer proximity of the gold center to the N_2 ligand and prevent phosphine abstraction by mitigating the steric relief driving force. The increased electron donating ability of depe also provides stronger phosphine metal bonds, although an increased electronic density at the metal center should also favor electron transfer reactions. In chlorobenzene-d_5 at RT, $\mathbf{3}_{W}$ reacted immediately with 1 equiv of **6b**$^+$, **6c**$^+$, **6d**$^+$ and **6e**$^+$ to form the corresponding heterobimetallic adducts $[W(N_2)(depe)_2(\mu\text{-}N_2)Au(NHC)][BAr^F]$ **10b–e**$_W$BAr^F as the main product, along with minor, unidentified paramagnetic compounds. In the same conditions, the reaction of **6a**BAr^F with $\mathbf{3}_{W}$ immediately gave an intractable mixture of products. The reactivity difference between **6a**$^+$ and **6b**$^+$ could originate from the electron donation of the methyl groups to the imidazole ring of **6b**$^+$, the resulting increased electronic density at the gold center in turn

disfavoring electronic transfers from the W center. Adducts **10b–e**$_w$BAr^F share similar spectroscopic signatures of which key parameters are summarized in Table 1. In ^{1}H NMR, adducts **10b–d**$_w$BAr^F are characterized by a single set of signals for the NHC ligand along with inequivalent methylene and ethyl fragments, indicative of a loss of symmetry at the W center. On the contrary, the NHC ligand of **10e**$_w$BAr^F shows differentiated signals in ^{1}H NMR for the substituents and the imidazole ring, which could be related to steric interactions between the depe ligand and the adamantyl moieties hindering free rotation on the NMR time scale. In all adducts, the phosphine ligands display a single, well resolved peak in ^{31}P{^{1}H} NMR, shifted upfield compared to **3**$_w$ ($\Delta\delta$: –1.6 to –3.6 ppm). As with adducts of dppe-supported complexes, the solution IR spectra of **10b–e**$_w$BAr^F display two broad bands corresponding to the elongated bridging dinitrogen in the 1700–1800 cm^{-1} region and the *trans* dinitrogen ligand in the 2000–2100 cm^{-1} region.

Table 1. Key NMR chemical shifts and vibrational modes of adducts 10b–e$_w$BAr^F **in solution.**

Complex	δ ^{31}P^a	$\Delta\delta$ ^{31}P *vs.* **3**$_w$^{a}	ν_{NN}^{b}	$\Delta\nu_{NN}$ *vs.* **3**$_w$^{b}
10b$_w$BAr^F	34.2	–2.0	1796	–113
			2044	+135
10c$_w$BAr^F	34.4	–1.8	1775	–134
			2050	+141
10d$_w$BAr^F	32.6	–3.6	1767	–142
			2052	+143
10e$_w$BAr^F	34.6	–1.6	1783	–126
			2048	+139

^{a}C$_6$D$_5$Cl, expressed in ppm. ^{b}C$_6$H$_5$Cl solution in transmission cell, expressed in cm^{-1}.

Isolation of heterobimetallic complexes 10b–e$_w$**BAr^F.** Complexes **10b–e**$_w$BAr^F decomposed within hours in solution as evidenced by the formation of broad signals along with multiples set of signals for the NHC ligands in ^{1}H NMR and the disappearance of ^{31}P NMR signals, both diagnostics of the formation of paramagnetic compounds (*vide infra*), presumably formed by W(0)

→ Au(I) electronic transfers. Nevertheless, **10b–e$_w$**BAr^F can be precipitated by pouring concentrated PhF solutions of the freshly formed adducts in precooled pentane (–40 °C) to afford purple to dark brown NaCl/**10b–e$_w$**BAr^F mixtures, recovered by decantation. The fine NaCl precipitate can then be suspended with pentane washes of the solids, allowing for the isolation of **10b–e$_w$**BAr^F as purple or brown microcrystalline powders in good yields (80–85%) (Scheme 6). The isolated adducts decompose slowly at room temperature and rapidly under vacuum but can be stored indefinitely at –40 °C. Characterization by elemental analysis gave a lower-than-expected N content, however this is likely the result of degradation during the analytical process as FTIR-ATR analysis confirmed the retention of the second N_2 ligand in the solid state.

Scheme 6. Isolation of heterobimetallic complexes 10b–e$_w$BAr^F **with relevant vibrational modes (ATR).**

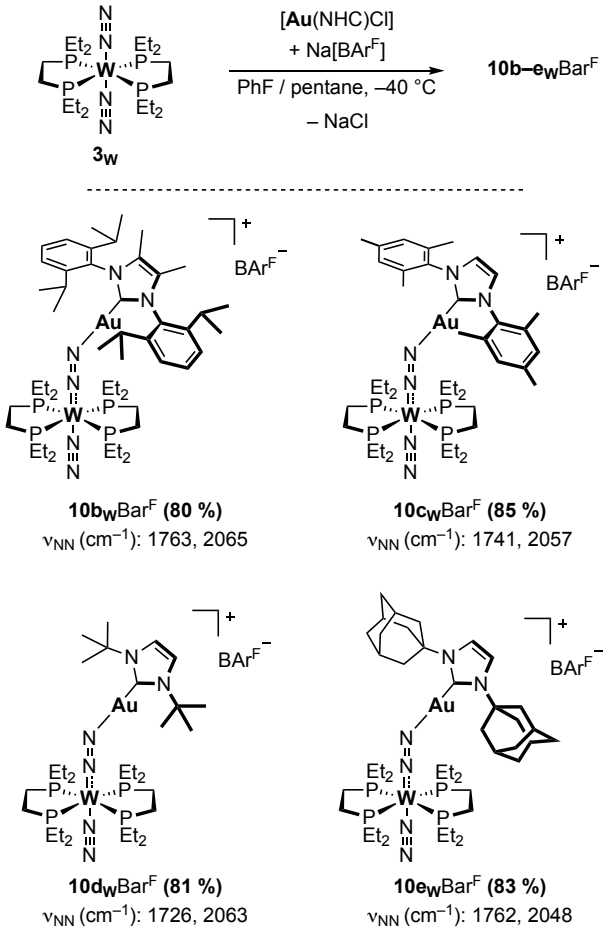

The bridging dinitrogen ligand is moderately activated in complexes **10b–e**$_w$BAr^F as evidenced by shifts in the vibrational frequencies ranging from –123 to –160 cm^{-1} (*vs.* **3**$_w$). Evaluation of the Lewis acidity of cations **6a**$^+$ to **6e**$^+$ yielded similar acceptor numbers (from **6a**$^+$ to **6e**$^+$, ANs = 87.3, 86.4, 87.5, 85.6, 85.3, see Table S2) for all NHC ligands, revealing that the variations of N_2 activation were mostly due to sterics. The percent buried volume ($\%V_{bur}$) is a good indication of the steric hindrance in the proximity of the gold center for symmetrical NHC ligands. According to the measured $\%V_{bur}$ on a series of [Au(Cl)(NHC)] complexes, cations **6**$^+$ can be ordered as **6d**$^+$ < **6e**$^+$ ≈ **6c**$^+$ < **6b**$^+$ by increasing steric hindrance ($\%V_{bur}$ = 44.4, 36.5, 39.8 and 39.6 % from **6b**$^+$ to **6e**$^+$, respectively).[43] However, the highest μ-N_2 ligand activation is achieved in the adduct **10d**$_w$BAr^F and differs significantly from adduct **10e**$_w$BAr^F, which indicates that long-range steric hindrance has

more impact than that in the gold center proximity. Indeed, the bulky, far-reaching adamantyl and diisopropylphenyl substituents of **6e**$^+$ and **6b**$^+$ translate to lower N_2 activation than when the planar mesityl or the smaller *tert*-butyl substituents found in **6c**$^+$ or **6d**$^+$, respectively, are present. No correlations were found between $\Delta\nu_{NN}$ and either the ANs of the cations or the $\%V_{bur}$.

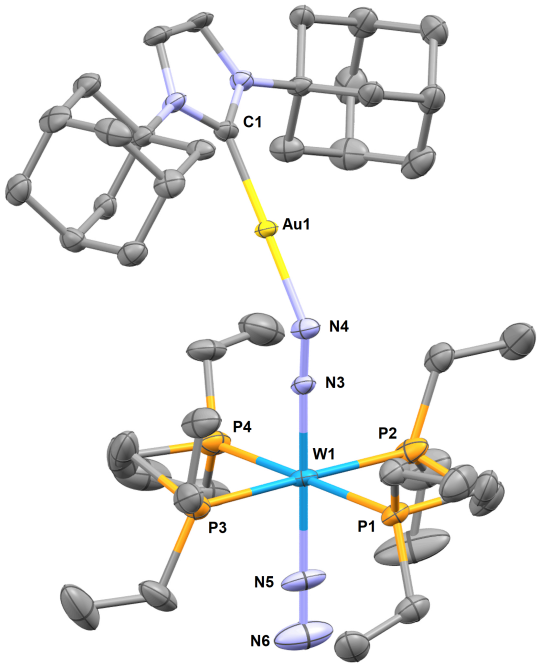

Figure 4. Molecular structure of complex **10e**$_w$BAr^F in the solid state (ellipsoids are drawn at the 50% probability level, hydrogen atoms are omitted for clarity). Selected bond lengths (Å) and angles (°): W1–N4 1.896(6), N4–N3 1.179(8), N3–Au1 2.015(6), W1–N5 2.071(7), N5–N6 1.09(1), W1–N4–N3 176.3(5), N4–N3–Au1 142.6(5), W1–N5–N6 177.4(7), N4–W1–N5 178.2(3), C1–Au1–N3 179.2(3).

The structure of **10e**$_w$BAr^F could be determined by single crystal X-ray diffraction analysis. This is, to the best of our knowledge, the first structural characterization of an N_2-bridged heterobimetallic complex featuring a group 11 metal. It features an octahedral ligand sphere

around the W center with two depe ligands included almost perfectly in the equatorial plan (Figure 4). The N_2 and μ-N_2 ligands are in axial position with a slight deformation to accommodate for the coordination of $[Au(IAd)]^+$ (N–W–N = 178.2(3) °). The W(μ-N_2)(Au{NHC}) motif presents a shortened W–N bond (1.896 Å vs. 2.0154(11) Å for $\mathbf{3}_w$) and a lengthened N–N bond (1.179 Å vs. 1.096 Å for free N_2 and 1.123(2) Å for $\mathbf{3}_w$). The bond orders are ambiguous with a W–N distance falling within simple and double bonds and the N–N distance within double and triple bonds.[44] The gold(I) complex unsurprisingly shows linear geometry with a N–Au bond distance of 2.015 Å, matching with the few examples of $[Au(NHC)]^+$ coordination to nitrogen bases (e.g., 2.016 Å for [(MeCN)Au(Idipp*)][BF_4]) with structural characterization.[45] The N–N–Au angle of 142.6 ° suggests a similar bonding situation as the one found in main group adducts of end-on dinitrogen complexes.[11e,12,46]

Comparison with relevant N_2-bridged adducts. To the best of our knowledge, there is only one example of a group 6 N_2 complex reacting with a Lewis acidic, d-block metal compound in the literature, to lead to the Mo(0)/Fe(II) heterobimetallic complex [(toluene)(PPh_3)$_2$Mo(μ-N_2)Fe(Cp)(dmpe)][BF_4] (dmpe = 1,2-bis(dimethylphosphino)ethane).[47] Its structure is however very similar to the numerous LA–TMs adducts reported with the d^6 *trans*-[ReCl(N_2)(PMe_2Ph)$_4$][6] complex, and they contrast strikingly with the $[Au(NHC)]^+$ adducts of $\mathbf{2}_w$ and $\mathbf{3}_w$. In typical adducts with a Lewis acidic metal M', the M–(μ-N_2)–M' core is essentially linear owing to the implication of empty or partially filled d-orbitals of M' in a four-center π molecular orbital.[48] Conversely, the structure of $\mathbf{10e}_w$$BAr^F$ has a bent W–(μ-N_2)–Au motif. Since this bonding situation is typically found with main group Lewis acids,[12] comparison of $[Au(NHC)]^+$ coordination to N_2 with boranes such as **1** is especially relevant. To this end, we have carried out the reaction of *trans*-[M(depe)$_2$(N_2)$_2$] (M = Mo $\mathbf{3}_{Mo}$, M = W, $\mathbf{3}_w$), with the strong LA tris(pentafluorophenyl)borane

($B(C_6F_5)_3$, **1**) in a similar fashion as reported previously with *trans*-[$M(dppe)_2(N_2)_2$] (**2**).[12] Upon treatment of complexes $\mathbf{3}_{Mo}$ and $\mathbf{3}_{W}$ with **1** in toluene-d_8 at room temperature, immediate formation of a dark brown solution was observed. The major product formed in both cases (> 75% for $\mathbf{3}_{Mo}$ and > 90% for $\mathbf{3}_{W}$ according to ^{31}P NMR) is the adduct *trans*-[$Mo(depe)_2(N_2)(N{=}N{-}B\{C_6F_5\}_3)$] ($\mathbf{11}_{Mo}$) or *trans*-[$W(depe)_2(N_2)(N{=}N{-}B\{C_6F_5\}_3)$] ($\mathbf{11}_{W}$) according to ^{1}H, ^{11}B, ^{19}F and ^{31}P NMR spectroscopy. The two compounds show similar spectroscopic signatures with two sets of signals for the ethyl groups and ethane backbone in ^{1}H NMR. The phosphines are equivalent as evidenced by a single peak in $^{31}P\{^{1}H\}$ NMR at δ = 52.9 ppm for $\mathbf{11}_{Mo}$ and δ = 34.7 ppm for $\mathbf{11}_{W}$ (J_{PW} = 293 Hz), upfield-shifted compared to $\mathbf{3}_{Mo}$ and $\mathbf{3}_{W}$ (δ = 55.9 and 36.2 ppm, respectively). Diagnostic signals of borane coordination are seen in ^{11}B and ^{19}F NMR. Layering pentane over toluene solutions of the complexes at –40 °C allows for their recovery as orange ($\mathbf{11}_{Mo}$) or purple ($\mathbf{11}_{W}$) crystals in 53% and 62% yield, respectively. The structures of complexes $\mathbf{11}_{Mo}$ and $\mathbf{11}_{W}$ were confirmed by X-Ray diffraction (Figure 5). The $M(\mu\text{-}N_2)(B\{C_6F_5\}_3)$ moiety features ambiguous bond orders with M–N distances falling within simple and double bonds [1.894(4) Å for $\mathbf{11}_{Mo}$ and 1.908(7) Å for $\mathbf{11}_{W}$ *vs*. 2.031 Å for $\mathbf{3}_{Mo}$ and ≈ 1.70–1.80 Å for M=N][49] and N–N distances for the bridging N_2 ligand falling within double and triple bonds [1.174(5) Å for $\mathbf{11}_{Mo}$ and 1.180(9) Å for $\mathbf{11}_{W}$ *vs*. 1.117 Å for $\mathbf{3}_{Mo}$ and 1.096 Å for free N_2]. The B–N bonds are comparable to adducts of **1** with other nitrogen bases [1.561(6) Å for $\mathbf{11}_{Mo}$ and 1.549(11) Å for $\mathbf{11}_{W}$].[50] The dinitrogen ligand in trans position shows longer M–N bonds [2.128(5) Å for $\mathbf{11}_{Mo}$ and 2.093(11) Å for $\mathbf{11}_{W}$]and shorter N–N distances [1.092(7) Å for $\mathbf{11}_{Mo}$ and 1.082(11) Å for $\mathbf{11}_{W}$] consistent with a decreased activation. The tetrahedral character of the boron atoms are 85% ($\mathbf{11}_{Mo}$) and 89% ($\mathbf{11}_{W}$).[51] FTIR-ATR spectra of the crystals feature two strong absorptions in the 2400–1600 cm^{-1} region, one corresponding to the stretching of the N–N bond of the bridging N_2 at 1789 cm^{-1} ($\mathbf{11}_{Mo}$) and 1767 cm^{-1} ($\mathbf{11}_{W}$) (*vs*. 1914 cm^{-1} for $\mathbf{3}_{Mo}$ and 1890 cm^{-1}

for $\mathbf{3}_{W}$); the second vibration corresponds to the stretching of the N–N bond of the monoligated N_2 ligand at 2120 cm^{-1} ($\mathbf{11}_{Mo}$) and 2076 cm^{-1} ($\mathbf{11}_{W}$).

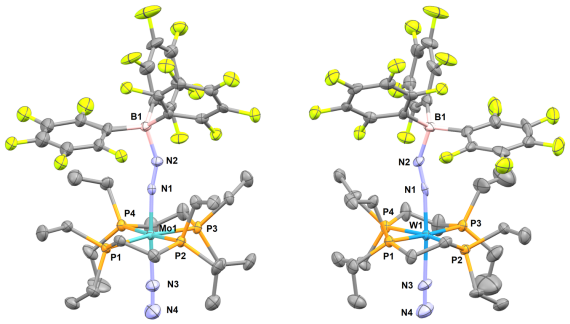

Figure 5. Molecular structure of complexes $\mathbf{11}_{Mo}$ (left) and $\mathbf{11}_{W}$ (right) in the solid state (ellipsoids are drawn at the 50% probability level; hydrogen atoms are omitted for clarity). Selected bond lengths (Å) and angles (°): $\mathbf{11}_{Mo}$: Mo1–N1 1.894(4), N1–N2 1.174(5), N2–B1 1.561(6), Mo–N3 2.128(5), N3–N4 1.092(7), Mo1–N1–N2 169.9(3), N1–N2–B1 150.9(4), Mo1–N3–N4 177.9(5), N1–Mo1–N3 176.26(16), C24–B1–C36 117.8(3), C24–B1–C30 111.4(3), C36–B1–C30 104.6(4), C24–B1–N2 105.1(3), C36–B1–N2 109.8(4), C30–B1–N2 107.8(4). $\mathbf{11}_{W}$: W1–N1 1.908(7), N1–N2 1.180(9), N2–B1 1.549(11), W–N3 2.093(8), N3–N4 1.082 (11), W1–N1–N2 168.9(5), N1–N2–B1 148.3(7), W1–N3–N4 177.9(8), N1–W1–N3 175.7(3), C31–B1–C41 112.7(7), C31–B1–C21 104.3(6), C41–B1–C21 114.9 (7), C21–B1–N2 109.8(7), C31–B1–N2 108.1(6), C41–B1–N2 106.9 (7).

The retention of the second N_2 ligand contrasts with the previously reported[12] structures of [Mo(dppe)$_2$(N=N–B{C_6F_5}$_3$)] ($\mathbf{12}_{Mo}$) and [W(dppe)$_2$(N=N–B{C_6F_5}$_3$)] ($\mathbf{12}_{W}$) for which the formation of the Lewis pair induced the dissociation of the second N_2 ligand. This retention is likely due to the electron richness of the depe ligand compared to the dppe ligand, which increases the electronic density available at the metal center for π-backbonding. The bridging N_2 ligand is slightly less

elongated in complexes $\mathbf{11}_{M}$ than in $\mathbf{12}_{M}$ as evidenced by shorter N–N distances (–0.02 to –0.03 Å). These differences correlate with the lower shift of the N–N stretching vibrations for $\mathbf{11}_{M}$ compared to $\mathbf{12}_{M}$ (*vs*. dinitrogen complexes $\mathbf{3}_{M}$) observed by FT-IR. Such a difference in N_2 activation can be attributed to the influence of the retained N_2 ligand, as d electrons involved in back-bonding are delocalized over two N_2 units in complexes $\mathbf{11}_{M}$.

Adducts of **1** or $\mathbf{6e}^{+}$ with $\mathbf{3}_{W}$ show similar N–N–LA angles (148.3 ° for $\mathbf{11}_{W}$, 142.6 ° for $\mathbf{10e}_{W}BAr^{F}$), elongations of the μ-N–N distance (1.180 Å for $\mathbf{11}_{W}$, 1.179 Å for $\mathbf{10e}_{W}BAr^{F}$) and shortening of the W–N bond (1.908 Å for $\mathbf{11}_{W}$, 1.896 Å for $\mathbf{10e}_{W}BAr^{F}$). This closeness in N_2 push-pull activation is in line with the ANs of LAs **1** and $\mathbf{6a–e}^{+}$, all being found between 79 and 88. The structural similarity between $\mathbf{11}_{W}$ and $[Au(NHC)]^{+}$ adducts of $\mathbf{3}_{W}$ is also reflected by their similar μ-N_2 vibrational frequencies, especially when compared to $\mathbf{10b}_{W}BAr^{F}$ and $\mathbf{10e}_{W}BAr^{F}$ ($\Delta\nu_{NN} \leq 5$ cm^{-1}). Although **1** and cation $\mathbf{6e}^{+}$ are poorly related in terms of structure, charge and electronegativity of their central element, their push-pull activation is comparable. Adducts $\mathbf{10c}_{W}BAr^{F}$ and $\mathbf{10d}_{W}BAr^{F}$ with the less bulky NHC substituents at gold afford greater N_2 activation than in $\mathbf{11}_{W}$. In regard to the similar properties of these $\mathbf{3}_{W}$ adducts, the predominant steric effect over the coordination of $[Au(NHC)]^{+}$ to N_2 complexes is unveiled by the considerable differentiation between $\mathbf{12}_{W}$ and the related gold adducts. Indeed, $\mathbf{12}_{W}$ presents a higher N_2 activation ($\Delta\nu_{NN}$ = –233 cm^{-1} *vs*. $\mathbf{2}_{W}$) than $\mathbf{11}_{W}$ whereas $[Au(NHC)]^{+}$ coordination on $\mathbf{2}_{W}$ leads to weaker N_2 activations than with $\mathbf{3}_{W}$ (e.g. $\Delta\nu_{NN}$ = –95 cm^{-1} *vs*. $\mathbf{2}_{W}$ for $\mathbf{7b}_{W}BAr^{F}$ and –124 cm^{-1} *vs*. $\mathbf{3}_{W}$ for $\mathbf{10b}_{W}BAr^{F}$). This difference of behaviors likely stems from the shape of the LAs as the NHCs' substituents expand toward the dppe ligands, which increases considerably the steric repulsion with the phenyl groups of the phosphine compared to the outward extending borane substituents. In addition, IR analyses of $\mathbf{2}_{W}$-gold adducts solutions point to a

retention of the second N_2 ligand which, as mentioned above, has an influence on the activation of the bridging N_2 ligand.

^{15}N-labeling experiments. The ^{15}N-labeled complexes ^{15}N-**10e$_w$**BAr^F and ^{15}N-**11$_w$** were synthesized from [W($^{15}N_2$)$_2$(depe)$_2$] (^{15}N-**3$_w$**) following the same aforementioned procedures. FTIR-ATR analysis of the labeled complexes confirmed the identification of the N_2 ligands vibration in the ^{14}N analogues with bathochromic shifts of –71 cm^{-1} (N_2) and –58 cm^{-1} (μ-N_2) for ^{15}N-**10e$_w$**BAr^F (*vs*. ^{14}N-**10e$_w$**BAr^F, bands at 1977 and 1704 cm^{-1}) and shifts of –69 cm^{-1} (N_2) and –58 cm^{-1} (μ-N_2) for ^{15}N-**11$_w$** (*vs*. ^{14}N-**11$_w$**, bands at 2076 and 1767 cm^{-1}). The ^{15}N NMR chemical shifts of ^{15}N-**10e$_w$**BAr^F and ^{15}N-**11$_w$** are reported in Table 2.

Table 2. NMR chemical shifts of adducts ^{15}N-10e$_w$BAr^F and ^{15}N-11$_w$.

Complex	Solvent	δ $^{15}N_\alpha$ (μ-N_2)[a]	δ $^{15}N_\beta$ (μ-N_2)[a]	δ $^{15}N_\alpha$ (N_2)[a]	δ $^{15}N_\beta$ (N_2)[a]
^{15}N-**2$_w$**	C_6D_6	-	-	–63.1	–52.0
^{15}N-**10e$_w$**BAr^F	C_6D_5Cl	–40.1	–119.0	–76.1	–42.9
^{15}N-**11$_w$**	C_6D_6	–55.0	–152.6	–73.9	–37.4

N_α = Atom adjacent to W; N_β = distal nitrogen. [a] Expressed in ppm.

Upon coordination of the Lewis acids, the terminal nitrogen (N_β) of the bridging N_2 is significantly shielded (–67 and –100.6 ppm for ^{15}**N-10e$_w$**BAr^F and ^{15}**N-11$_w$** respectively) while the tungsten bound nitrogen (N_α) is slightly deshielded (–23 and –8.1 ppm for ^{15}**N-10e$_w$**BAr^F and ^{15}**N-11$_w$** respectively) compared to ^{15}**N-2$_w$**. A similar trend was observed by Donovan-Mtunzi *et al*[52] upon

coordination of $AlMe_3$ on various dinitrogen complexes, which contrasts with transition-metal acceptors that typically induce a deshielding of N_β.

Computational Studies. In order to get insight into the nature of the μ-N_2–$B(C_6F_5)_3$ and μ-N_2–$[Au(NHC)]^+$ bonds and into the impact of the exogenous LAs on the electronic structure of the M(group 6)-N_2 unit, we carried out a DFT computational study at the B3PW91 level of theory on the *trans*-$[W(depe)_2(N_2)(N{=}N{-}B\{C_6F_5\}_3)]$ (**11**$_w$) and *trans*-$[W(depe)_2(N_2)(\mu\text{-}N_2)Au(IAd)][BAr^F]$ (**10e**$_w$$BAr^F$) complexes. The optimized structures of **11**$_w$ (**11**$_{w\text{-}opt}$) and **10e**$_w$$BAr^F$ (**10e**$_w$$BAr^F{}_{\text{-opt}}$) are shown in Figure 6. Their corresponding bond distances and angles are listed in Table 3 and compared with those observed experimentally for **11**$_w$ and **10e**$_w$$BAr^F$ as well as with those of the $[W(depe)_2(N_2)_2]$ precursor (**3**$_w$ and **3**$_{w\text{-}opt}$).

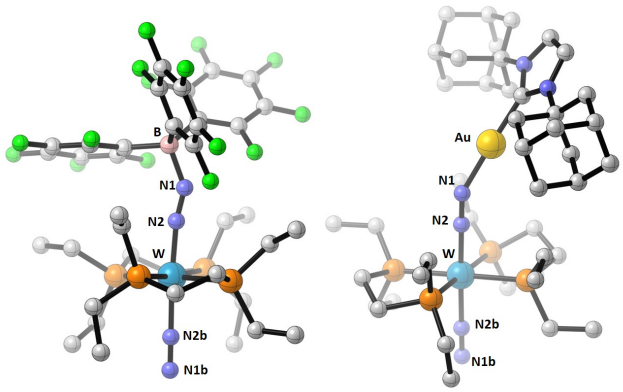

Figure 6. DFT-optimized molecular structures of complexes **11**$_{w\text{-}opt}$ (left) and **10e**$_w$$BAr^F{}_{\text{-opt}}$ (right). The hydrogen atoms and the $[BAr^F]^-$ anion have been omitted for the sake of clarity.

Table 3. Significant bond distances (Å) and angles (°) for **10e**$_w$$BAr^F$, **10e**$_w$$BAr^F{}_{\text{-opt}}$, **11**$_w$, **11**$_{w\text{-}opt}$, **3**$_w$ and **3**$_{w\text{-}opt}$.

	W-N2	N2-N1	N1-LA	W-N2b	N2b-N1b	W-N2-N1	N2-N1-LA	W-N2b-N1b

11$_{W}$	1.908	1.179	1.550	2.094	1.082	169.0	148.4	177.9
11$_{W\text{-}opt}$	1.892	1.169	1.552	2.055	1.128	170.7	145.5	179.1
10e$_{W}$BAr^{F}	1.896	1.179	2.015	2.071	1.093	176.3	142.6	177.4
10e$_{W}$BAr^{F}$_{opt}$	1.905	1.169	2.002	2.048	1.129	178.4	148.8	177.4
3$_{W}$	2.015	1.123	-	2.015	1.123	178.6	-	178.6
3$_{W\text{-}opt}$	1.999	1.139	-	2.000	1.138	178.3	-	178.3

As shown in Table 3, the computed bond distances and angles accurately reproduce the values obtained experimentally with variations that fall within the error of the DFT method. In accordance with the experimental results, the W(μ-N_2)–(LA) motif presents a shortened W–N2 bond (1.892 and 1.905 Å for **11**$_{W\text{-}opt}$ and **10e**$_{W}$BAr^{F}$_{opt}$, respectively, compared to 2.000 Å for **3**$_{W\text{-}opt}$) and a lengthened N1–N2 bond (1.169 Å for both **11**$_{W\text{-}opt}$ and **10e**$_{W}$BAr^{F}$_{opt}$, compared to 1.139 Å for **3**$_{W\text{-}opt}$). The N2–N1–LA angles, in addition, measure 145.5 ° for **11**$_{W\text{-}opt}$ and 148.8 ° for **10e**$_{W}$BAr^{F}$_{opt}$, reproducing well the bent structure observed in the corresponding crystallized complexes. In order to discard the possible implication of solely steric effects in the formation of these bent structures, such as, in particular, the steric constraint between the LA ligands and the diphosphine substituents, we computed the **11**$_{W\text{-}opt}$ compound by replacing the pentafluorophenyl groups by trifluoromethyl ones (**13**$_{W\text{-}opt}$), and the **10e**$_{W}$BAr^{F}$_{opt}$ complex, by replacing the adamantyl groups with methyl ones (**14**$_{W\text{-}opt}$$^{+}$). As shown in Figure S94, both the new structures display acute N–N–LA angles (139.0 ° for **13**$_{W\text{-}opt}$ and 131.8 ° for **14**$_{W\text{-}opt}$), pointing out that the main reason for the observed bent geometry must not be attributed to sterically induced repulsions, but rather to electronic factors. The computed Wiberg bond indexes (Table S12) are in accordance with the experimental and computed geometrical parameters. While for the N2–N1 bond the Wiberg indexes decrease from 2.52 (**3**$_{W\text{-}opt}$) to 2.10 (**10e**$_{W}$BAr^{F}$_{opt}$) to 2.04 (**11**$_{W\text{-}opt}$), for the W–N2 bond, on the other hand, they increase, from 0.97 (**3**$_{W\text{-}opt}$)

to 1.28 (**10e**$_{W}$BAr$^{F}_{-opt}$) to 1.33 (**11**$_{W-opt}$). This LA-induced N_2 activation correlates well with the lower energies found for the computed μ-N–N asymmetric stretching vibrations of **11**$_{W-opt}$ and **10e**$_{W}$BAr$^{F}_{-opt}$ (1904 and 1880 cm^{-1}, respectively) compared to **3**$_{W-opt}$ (2011 cm^{-1}).

Considering a valence bond approach, the bonding situation in complexes **11**$_{W-opt}$ and **10e**$_{W}$BAr$^{F}_{-opt}$ falls between two extremes, that are on one side a linear W–N2–N1–LA geometry with the N1 atom *sp* hybridized in a borata- or auryl-diazenium ligand and on the other side a W–N2–N1–LA bent geometry with the N1 atom sp^2-hybridized in a borata- or auryl diazenido ligand (Figure 7).[53]

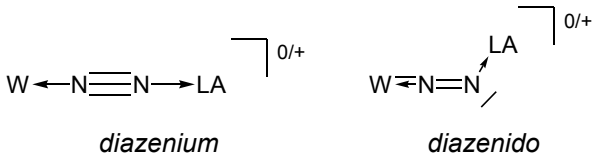

Figure 7. Lewis structures extrema for **11**$_{W}$ and **10e**$_{W}^{+}$: diazenium *vs*. diazenido ligand.

To shed light on this ambiguous situation, we computed the molecular orbitals of compounds **11**$_{W-opt}$ and **10e**$_{W}$BAr$^{F}_{-opt}$. For complex **11**$_{W-opt}$, while the HOMO is essentially nonbonding at tungsten (Figure S95), the energetically close HOMO–1 and HOMO–2 orbitals show a strong back-bonding donation from a filled W(depe)$_2$ *d* orbital to an unfilled N_2 π* orbital, displaying a significant W–N π-bonding character, indicative of a multiple bonding between the W and the N2 atom (Figure 8).

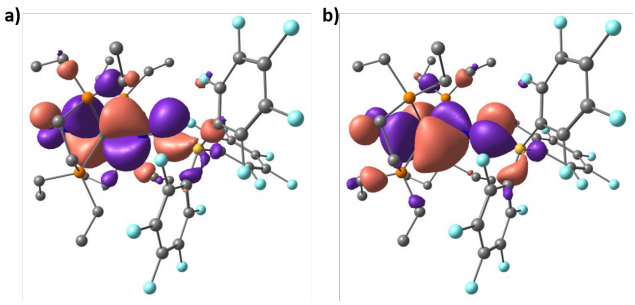

Figure 8. DFT-computed molecular orbitals of complex $\mathbf{11}_{W\text{-}opt}$: (a) HOMO-1; (b) and HOMO-2.

While in the HOMO-1 orbital, the back-bonding donation involves the W(depe)$_2$ *d* and the N_2 π* orbitals which are perpendicular to the N2–N1–B plane, in the HOMO-2 orbital, on the other hand, the back-bonding donation involves the W(depe)$_2$ *d* and N_2 π* orbitals which are coplanar to the N–N–B plane. In both the HOMO–1 and HOMO–2 molecular orbitals, interestingly, an overlap between a μ-N_2 π* lobe and a B sp^3 orbital is observed. As described by Szymczak *et al.*,[11e] this interaction is likely to lower the energy of the π* orbital in N_2, leading to an augmented back-bonding donation from the W(depe)$_2$ fragment. In compound $\mathbf{11}_W$, therefore, the presence of a bent rather than linear N2–N1–B bond angle (148.4 ° and 145.5 ° in $\mathbf{11}_W$ and $\mathbf{11}_{W\text{-}opt}$, respectively), maximizes the overlap between the B sp^3 orbital and a lobe of the μ-N_2 π* orbital, the extent of the N2–N1–B bending being likely correlated with the steric properties of the boron substituents. Akin to $\mathbf{11}_{W\text{-}opt}$, the HOMO of $\mathbf{10e}_W\text{BAr}^F{}_{opt}$ is essentially a tungsten-localized nonbonding orbital (Figure S95), whereas the HOMO-1 and HOMO-2 show the back-bonding donation from the W(depe)$_2$ to the N_2 unit, with a significant W–N π-bonding character reflecting a multiple bonding between the W and the N2 centers (Figure 9). It is worth underlining here that the nonbonding nature of the HOMO *d* orbital in both $\mathbf{10e}_W\text{BAr}^F{}_{opt}$ and $\mathbf{11}_{W\text{-}opt}$ strongly evokes the electronic structure of the $SiMe_3^+$ adduct of the iron(0) dinitrogen complex [Fe(N_2)(depe)$_2$] computed by the group of Ashley.[46] Like in compound $\mathbf{11}_{W\text{-}opt}$, the HOMO–1 and HOMO–2 orbitals of complex $\mathbf{10e}_W\text{BAr}^F{}_{opt}$ (Figure 9) involve the W(depe)$_2$ *d* and the N_2 π* orbitals which are perpendicular and coplanar to the N2–N1–Au plane, respectively. In the HOMO–2 orbital, interestingly, one lobe of the μ-N_2 π* orbital overlaps with a lobe of the Au^+ *sd* vacant orbital, partially contributing to the N1–Au^+ bond interaction. In contrast with compound $\mathbf{11}_{W\text{-}opt}$ in which both the HOMO–1 and HOMO–2 orbitals are bonding with respect to the N1–LA bond, in $\mathbf{10e}_W\text{BAr}^F{}_{opt}$ this is the case for only the HOMO–2 since the HOMO–

1 orbital displays an antibonding N1–Au^{+} interaction (Figure S96). This, added to the fact that the overlap between the Au^{+} *sd* orbital with the π* orbital of μ-N_2 is not optimal, may account for the experimentally observed higher lability of the N_2 gold adduct compared to the N_2 boron analogue.

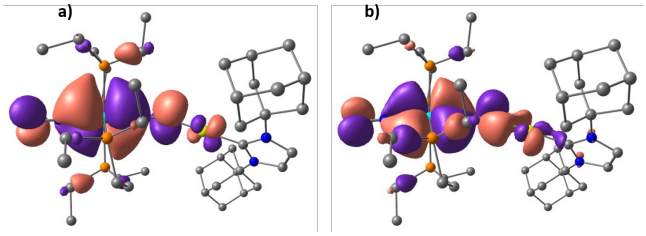

Figure 9. DFT calculated molecular orbitals of complex **10e**$_w$BAr$^{F}_{-opt}$: (a) HOMO-1 and (b) HOMO-2. The [BAr^{F}]$^{-}$ anion has been omitted for clarity.

In the HOMO-2 orbital of **10e**$_w$BAr$^{F}_{-opt}$, in addition, the same Au^{+} *sd* orbital which overlaps with the N_2 π* orbital is in turn involved in a π-backbonding donation with the *p* orbital of the carbenic carbon atom. Over recent years, the π-acceptor ability of NHCs in gold(I) complexes has received considerable attention with several experimental and theoretical studies aimed at characterizing it.[54] As shown in Figure 10, indeed, the vacant Au^{+} *sd* orbital is likely to interact at the same time with i) the π* orbital of the bridging N_2 molecule and ii) the *p* orbital of the carbon atom of the NHC ligand. In the HOMO-2 orbital, interestingly, the bent N–N–Au geometry (142.6° and 148.8 ° in **10e**$_w$BAr^{F} and **10e**$_w$BAr$^{F}_{-opt}$ respectively) allows the Au^{+} *sd* orbital to improve the overlap with a lobe of the μ-N_2 π* orbital, providing a push-pull force in the N_2 activation process.

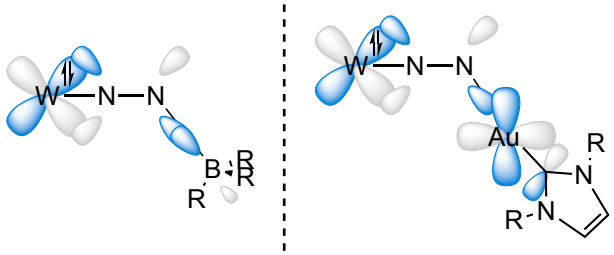

Figure 10. Simplified frontier orbital depiction accounting for the W–N–N–LA bonding interaction with localized MOs.

In order to get a deeper insight into the nature of this μ-N_2 π* - Au^+ *sd* interaction, we decided to compare the molecular orbitals of **10e**$_w$BAr$^F_{-opt}$ with those of the corresponding [W(depe)$_2$(N_2)$_2$] (**3**$_{W-opt}$) and [(N_2)Au(IAd)]$^+$ fragments. As shown in Figure 11, the HOMO-2 orbital of **3**$_{W-opt}$ displays a strong back-bonding donation from a filled W(depe)$_2$ *d* orbital to an unfilled N_2 π* orbital, like the one observed in the HOMO-2 orbital of the **10e**$_w$BAr$^F_{-opt}$ complex. The [(N_2)Au(IAd)]$^+$ fragment, on the other hand, displays a linear N–N–Au^+ geometry, which reflects the presence in its LUMO of an unfilled N_2 π* orbital. A careful analysis of this LUMO orbital shows an antibonding interaction between the unfilled N_2 π* orbital and the vacant Au^+ *sd* coplanar orbital. When the [W(depe)$_2$(N_2)] and [(N_2)Au(IAd)]$^+$ fragments interact, the W(depe)$_2$ *d* orbital may fill by back-bonding donation the N_2 π* orbital of the [(N_2)Au(IAd)]$^+$ cation, inducing a bend in the N–N–Au^+ angle. This N–N–Au^+ bent geometry may thus allow a partial overlap of the filled N_2 π* and the vacant Au^+ *sd* orbitals, the N_2 π* - Au^+ *sd* interaction switching from antibonding to partially bonding.

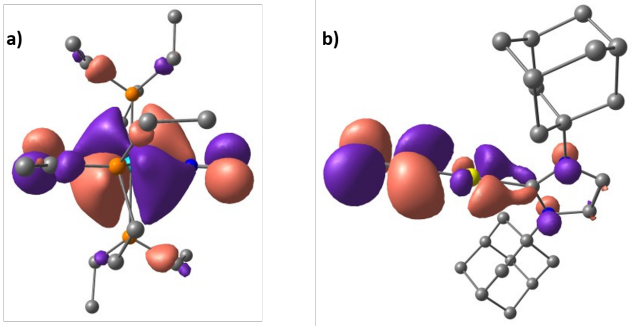

Figure 11. DFT calculated molecular orbitals of the [W(depe)$_2$(N_2)$_2$] and [(N_2)Au(IAd)]$^+$ fragments: (a) HOMO-2 of the [W(depe)$_2$(N_2)$_2$] moiety; (b) LUMO of the [(N_2)Au(IAd)]$^+$ cation.

The frontier orbitals reflect therefore a partial sp^2 hybridization of the N1 atom, underlining the predominance of the borata- or auryl diazenido form in Figure 9, due to the LA-induced push-pull effect. A careful analysis of the deeper orbitals has shown that other types of orbital overlaps also account for the N1–LA bond (Figures S97 and S98). These interactions, however, do not allow an understanding of the origin of the N2–N1–LA distortion, which is mainly related to the filling of the μ-N_2 π* orbital occurring in the frontier orbitals. Another proof of the LA-induced N_2 activation is given by the increase of μ-N_2 polarization as attested by the natural charges computed *via* a NBO analysis (Table S13). Importantly, and in line with the results of Szymczak and co-workers,[11e] the negative charge of the μ-N_2 terminal nitrogen (N1) increases from –0.1 in $\mathbf{3}_{W\text{-}opt}$ to –0.19 in $\mathbf{11}_{W\text{-}opt}$ to –0.35 in $\mathbf{10e}_W BAr^F{}_{\text{-}opt}$, and so does the N1–N2 charge difference from $\Delta_{N1-N2} = 0.015$ in $\mathbf{3}_{W\text{-}opt}$ to 0.31 in $\mathbf{11}_{W\text{-}opt}$ and to 0.45 in $\mathbf{10e}_W BAr^F{}_{\text{-}opt}$. In the latter compound, interestingly, the much higher negative charge on the μ-N_2 terminal nitrogen (N1) suggests that an electrostatic contribution may also account for the N1–Au^+ interaction. We have therefore embarked on the calculation of the natural charge of the entire LA acceptor fragment for complexes $\mathbf{11}_{W\text{-}opt}$ and $\mathbf{10e}_W BAr^F{}_{\text{-}opt}$ and we have estimated the force of the electrostatic interaction by comparing the charge separation between the μ-N_2 terminal atom (N1) and the whole LA acceptor group. While the natural charge of the $B(C_6F_5)_3$ group in complex $\mathbf{11}_{W\text{-}opt}$ amounts –0.44, that of the Au^+–NHC unit in complex $\mathbf{10e}_W BAr^F{}_{\text{-}opt}$ measures 0.63, providing in the latter a charge separation between the terminal N1 atom and the Au^+–NHC moiety of $\Delta_{N1\text{-}L_A} = 1.00$. This high level of polarization indicates that the μ-N_2–Au^+ bond has an important electrostatic component which may in part explain the undesired redox events that have lead in some instances to Au(0) and paramagnetic W species (*vide supra*).

Reactivity study of $[W(N_2)(depe)_2(\mu\text{-}N_2)Au(NHC)]^+$ adducts in solution and isolation of a tungsten decomposition product. To assess whether the rapid decomposition of complexes **10b–e**$_w$BAr^F precluded their use in dinitrogen transformation reactions, we formed the adducts *in situ* in chlorobenzene-d_5 and added immediately 1 equiv of unsaturated organic substrates of various natures at RT, having in mind to exploit the carbophilic properties of gold to promote N_2 functionalization via N–C bond formation. According to NMR and GC-MS analysis of the solution, 2-butyne, 3-methyl-1,2-butadiene or diisopropylcarbodiimide did not react while the adducts decomposed to mixtures of paramagnetic materials. Surprisingly, under the same conditions we observed a deuteration of the olefinic protons of 1-octene with full deuteration of the hydrogen atom in the 2-position and partial deuteration at the 1-position after 18 h at RT with **10d**$_w$BAr^F, as evidenced by ^{1}H NMR spectroscopy and GC-MS analysis (most abundant ion: 113.13 m/z = 1-octene + 1). Up to 20 equiv of 1-octene can be deuterated in the presence of **10d**$_w$BAr^F at RT in cholorobenzene-d_5, with 90% and 35% conversion of the 2- and 1-positions, respectively, after 5 days. While neither **3**$_w$ nor gold cations alone react with 1-octene, the H/D exchange is unlikely to be catalyzed by the adducts considering that the activity of the reaction is unrelated to the evolution of the adducts' concentration as they decompose.

Attempts to isolate or characterize the species formed from the decomposition of the gold adducts in the presence of the organic substrate have been mostly unsuccessful at the exception of the dinuclear salt $[\{W(Cl)(depe)_2\}_2(\mu\text{-}N_2)][BAr^F]_2$ formed in *ca.* 40% yield (relative to W content) as deep green crystals precipitating out of the reaction solutions over a period of days in the presence of 3-methyl-1,2-butadiene or diisopropylcarbodiimide. While sufficient to identify this species with good confidence, the low quality of these crystals did not allow for a full structural resolution by X-ray diffraction analysis and their very poor solubility in usual solvent hindered

recrystallization attempts. In the presence of organic substrates, isolated adduct **10d**$_w$BAr^F solubilized in chlorobenzene at RT afforded the W(II) complex in similar yield to that for adducts formed *in situ* from the reaction of **3**$_w$ with Na[BAr^F] and [Au(Cl)(NHC)], such a result would suggest that the chloride atoms originate from chlorobenzene. To strictly rule out the sourcing of the chloride ligand from trace amount of NaCl, we synthesized [Au(NTf$_2$)(Me$_2$Idipp)] (**6b**NTf$_2$), following a literature procedure.[30] This complex reacts immediately with 1 equiv of **3**$_w$ at RT in chlorobenzene-d_5 to afford [W(N$_2$)(depe)$_2$(μ-N$_2$)Au(Me$_2$Idipp)][NTf$_2$] **10b**$_w$NTf$_2$, characterized in solution by almost identical ^{1}H and ^{31}P NMR and IR (ν_{NN} = 1796 cm^{-1} in PhCl) spectroscopic signatures to those of **10b**$_w$BAr^F. By contrast, reaction of **6b**NTf$_2$ with **2**$_w$ affords only a minor quantity of the putative adduct [W(N$_2$)(dppe)$_2$(μ-N$_2$)Au(Me$_2$Idipp)][NTf$_2$] as the displacement of the more coordinating NTf$_2$ anion by **2**$_w$ is very slow (< 20% after 24 h) and evolves to a mixture of paramagnetic materials upon longer reaction times or a temperature increase to 45 °C.

In chlorobenzene, **10b**$_w$NTf$_2$ decomposes to an intractable mixture from which deep green crystals had formed after two days at RT. Structural determination by X-ray diffraction allowed the identification of these green crystals as the complex [{W(Cl)(depe)$_2$}$_2$(μ-N$_2$)][NTf$_2$]$_2$ (**15**$_w$[NTf$_2$]$_2$). In contrast with its [BAr^F]$^-$ counterpart, decomposition of **10b**$_w$NTf$_2$ led to the formation of these characteristic green crystals even in absence of organic substrates; the weakly coordinating NTf$_2$ anion is therefore assumed to play a similar role to the weakly coordinating organic substrates in the decomposition process. The homobimetallic dication [{W(Cl)(depe)$_2$}$_2$(μ-N$_2$)]$^{2+}$ depicted in Figure 12 features a linear (Cl–W)$_2$(μ-N$_2$) motif with short W–N distances (1.815(5), 1.804(5) Å) and a long N–N bond length (1.273(7) Å) that are almost identical to the dimension of the previously reported {Cp*W[N(^{i}Pr)C(Me)N(^{i}Pr)]}$_2$(μ-N$_2$)[55] and consistent with an electronic

configuration lying somewhere between a pair of W(II) centers bridged by an activated $(N_2)^0$ ligand and a pair of W(IV) centers bridged by a $(N_2)^{4-}$ group.

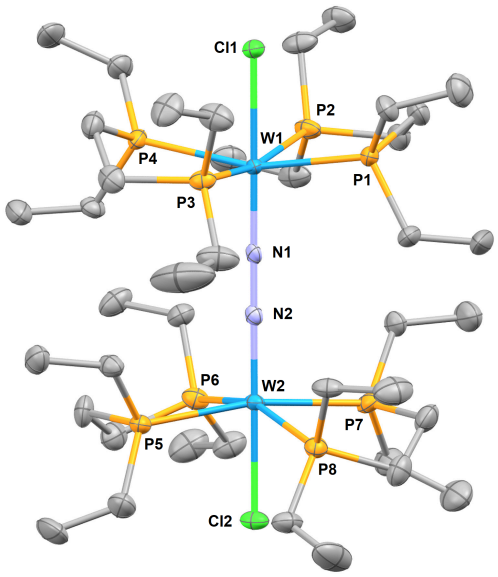

Figure 12. Molecular structure of $[\{W(Cl)(depe)_2\}_2(\mu\text{-}N_2)]^{2+}$ (**15**$_w^{2+}$) in the solid state (ellipsoids are drawn at the 50% probability level, hydrogen atoms and NTf_2 anions are omitted for clarity). Selected bond lengths (Å) and angles (°): W1–Cl1 2.4550(16), W1–N1 1.816(5), N1–N2 1.272(7), W2–N2 1.805(5), W2–Cl2 2.4663(16), Cl1–W1–N1 179.34(18), N2–W2–Cl2 178.93(18), W1–N1–N2 179.0(5), W2–N2–N1 179.3(5).

Evidently, the formation of **15**$_w[NTf_2]_2$ from **10b**$_w NTf_2$ results from the activation of chlorobenzene; this assumption can be confirmed by GC-MS analysis of the mixture after the formation of **15**$_w[NTf_2]_2$ allowing the identification of the major organic residue present in solution as isomers of chlorobenzene coupling compounds Ph-Ph, Ph-C_6H_4Cl and C_6H_4Cl-C_6H_4Cl (see the Supporting Information pp 8–9). A plausible explanation for such observation could be the initial oxidation of the W center by the gold cation followed by the generation of aryl radicals. However, the formation

of multiple paramagnetic materials resisting the characterization attempts and Au(0) propensity to form nanoparticles did not allow us to make any meaningful proposition regarding the mechanism responsible for the formation of biaryls and $\mathbf{15}_{W}[NTf_2]_2$.

Summary and Conclusions. To assess whether gold's well-known carbophilicity could be exploited to promote new transformation of N_2, the coordination properties and electronic compatibility of [Au^{I}(NHC)] cations with zerovalent group 6 dinitrogen complexes *trans*-[M(dppe)$_2$(N$_2$)$_2$] ($\mathbf{2}_{M}$), *trans*-[M(depe)$_2$(N$_2$)$_2$] ($\mathbf{3}_{M}$) and [M(PMe$_2$Ph)$_4$(N$_2$)$_2$] ($\mathbf{4}_{M}$) were explored (M = Mo or W). Unprecedented M(μ-N$_2$)–Au^{+} Lewis pairs have been observed by spectroscopic methods. Heterobimetallic complexes [W(N$_2$)(dppe)$_2$(μ-N$_2$)Au(NHC)][BAr^{F}] [NHC = Idipp ($\mathbf{7a}_{W}$BAr^{F}); Me$_2$Idipp ($\mathbf{7b}_{W}$BAr^{F})] and [W(N$_2$)(depe)$_2$(μ-N$_2$)Au(NHC)][BAr^{F}] [NHC = Me$_2$Idipp ($\mathbf{10b}_{W}$BAr^{F}); IMes ($\mathbf{10c}_{W}$BAr^{F}); I^{t}Bu ($\mathbf{10d}_{W}$BAr^{F}); IAd ($\mathbf{10e}_{W}$BAr^{F})] have been obtained from the reaction of the N$_2$ complex with the appropriate [Au(NHC)] cation generated *in situ* from [Au(Cl)(NHC)] and Na[BAr^{F}] and could be isolated in satisfying yields and purity, while the adducts formed with the Mo complexes have shown poor solution stability, precluding isolation. Indeed, the formation of the targeted gold adducts have been shown to be in competition with multiple side reactions, resulting in short-lived adducts in most conditions and an extreme sensitivity of the few characterizable heterobimetallic complexes discussed in this study. Gold coordination to N$_2$ is weaker than that to phosphines, which results readily in phosphine abstraction to form heteroleptic gold complexes, driven by either the relief of steric crowding or weak coordination to the group 6 metal and favored when the gold center bears low steric bulk. These reactions can be mitigated by the use of chelating phosphines and/or bulky NHCs but are responsible nevertheless for the lack of long-lived characterizable molybdenum complexes, whose coordination by phosphines is weaker than tungsten. The use of a bulky substituent at gold's NHC ligand can lead to weak N$_2$

coordination as seen with **7a**$_w$BAr^F and **7b**$_w$BAr^F that readily decompose to *trans*-[W(dppe)$_2$(N$_2$)$_2$] as a result of gold dissociation and subsequent decomposition. Likewise, the use of the more electron donating depe ligands for the dinitrogen complex prevents gold dissociation as a result of a more electron-rich N_2 ligand. However, this also favored electron transfers from the group 6 metal to the gold cations to lead gradually to mixtures of paramagnetic materials. In the sufficiently long-lived adducts **7a—b**$_w$BAr^F and **10a–e**$_w$BAr^F, the push-pull activation of the bridging N_2 ligand is weak to moderate as characterized by the $\Delta\nu_{NN}$ ranging from –95 cm^{-1} to –160 cm^{-1}, with higher degrees of N–N bond weakening found when the least hindered gold cation was employed.

For comparative purposes, adducts **11**$_M$ of the depe-supported **3**$_M$ complexes with the strong, archetypical boron Lewis acid B(C$_6$F$_5$)$_3$ (**1**) have been prepared and fully characterized. Especially relevant is the comparison of the structurally characterized heterobimetallic complex [W(N$_2$)(depe)$_2$(μ-N$_2$)Au(IAd)][BAr^F] (**10e**$_w$BAr^F) with **11**$_w$. As judged by $\Delta\nu_{NN}$ gained from IR spectroscopy, the level of push-pull activation of the bridging N_2 ligand is comparable and moderate (**10e**$_w$BAr^F: –126 cm^{-1}, **11**$_w$: –123 cm^{-1} *vs*. **3**$_w$). Solid-state molecular structures of **10e**$_w$BAr^F and **11**$_w$ both show a bent N–N–LA motif, with similar angles of 143 ° and 148 °, respectively, and identical N–N bond elongations (*ca*. +0.05 Å). This similarity of gold with a main group Lewis acid[14,56] must be qualified in light of the DFT calculations. They have shown that while in the presence of the boron LA, the μ-N$_2$–LA bond formation involves the mixing of μ-N$_2$ π* orbitals with *sp*^{3} hybrid orbitals at boron, in the gold case, a μ-N$_2$ π* orbital mixes with an *sd* hybrid orbital located at the gold center. In the Au$^+$ adduct, interestingly, the vacant *p* orbital of the ancillary NHC ligand also participates in this μ-N$_2$π* - Au$^+$ *sd* bonding interaction. The natural charges computed *via* an NBO analysis indicate that the charge separation between the terminal N1 atom and the Au$^+$–NHC moiety is larger than the one between the former and the B(C$_6$F$_5$)$_3$ group, suggesting an

important electrostatic component in the μ-N_2–[Au(NHC)]$^+$ bond. For both compounds, finally, the presence of a bent rather than linear N–N–LA bond angle (148.4 ° and 142.6 ° in $\mathbf{11}_w$ and $\mathbf{10e}_w$$BAr^F$, respectively), maximizes the overlap between a lobe of the μ-N_2 π* orbital and either a B sp^3 orbital ($\mathbf{11}_w$) or the Au^+ *sd* orbital, the extent of the N–N–LA bending being likely correlated with the steric properties of the LA substituents. The lower μ-N_2 π* – Au^+ *sd* bonding overlapping, compared to the μ-N_2 π* - B sp^3 interaction, is compensated by a more important electrostatic character for the μ-N_2–Au^+ bonding than for the μ-N_2–B one. This may therefore explain why gold coordination results ultimately in similar effects to those of $B(C_6F_5)_3$ complexation.

Preliminary reactivity experiments on the few stable gold adducts with unsaturated organic substrates lead in most conditions to the recovery of the latter and the formation of a mixture of paramagnetic materials among which [{W(Cl)(depe)$_2$}$_2$(μ-N_2)][BAr^F]$_2$ ($\mathbf{15}_w$[BAr^F]$_2$) could be identified. This bridged tungsten dication can be isolated under the same conditions from [W(N_2)(depe)$_2$(μ-N_2)Au(NHC)][NTf_2] ($\mathbf{15}_w$[NTf_2]$_2$) solutions, the chloride ligand being sourced under an unknown mechanism from chlorobenzene, of which coupling products have been identified by GC-MS analysis. These reactions were accompanied by H/D exchange reactions of 1-octene olefinic protons. Although the mechanisms and active species of these transformations are unknown, the heterobimetallic adducts are unlikely to be involved. The sum of these observations is indicative of a redox incompatibility between gold(I) complexes and group 6 metals which preclude their combined use in the envisioned gold promoted N_2 reactivity with unsaturated C–C bonds. Exploration of less reductive Re^I–N_2complexes is a possible development to mitigate electronic transfers.

ASSOCIATED CONTENT

Supporting Information.

The Supporting Information is available free of charge at https://pubs.acs.org/doi/10.1021/acs.inorgchem.0c03271.

Spectroscopic characterization and additional experimental protocols, figures and tables, cartesian coordinates from crystallography data and cartesian coordinates of all optimized stationary points.

Accession Codes

CCDC 2009824-2009828, 2036361 and 2054787 contain the supplementary crystallographic data for this paper. These data can be obtained free of charge via www.ccdc.cam.ac.uk/data_request/cif, or by emailing data_request@ccdc.cam.ac.uk, or by contacting The Cambridge Crystallographic Data Centre, 12 Union Road, Cambridge CB2 1EZ, UK; fax: +44 1223 336033.

AUTHOR INFORMATION

Corresponding Author

Antoine Simonneau — LCC-CNRS, Université de Toulouse, CNRS, UPS, 205 route de Narbonne, BP44099, F-31077 Toulouse cedex 4, France; orcid.org/0000-0003-4612-284X; Email: antoine.simonneau@lcc-toulouse.fr

Chiara Dinoi — LPCNO, CNRS & INSA, Université Paul Sabatier, 135 Avenue de Rangueil, 31077 Toulouse, France; Email: cdinoi@insa-toulouse.fr

Authors

David Specklin — LCC-CNRS, Université de Toulouse, CNRS, UPS, 205 route de Narbonne, BP44099, F-31077 Toulouse cedex 4, France; Email: david.specklin@lcc-toulouse.fr

Anaïs Coffinet — LCC-CNRS, Université de Toulouse, CNRS, UPS, 205 route de Narbonne, BP44099, F-31077 Toulouse cedex 4, France; Email: anais.coffinet@lcc-toulouse.fr

Laure Vendier — LCC-CNRS, Université de Toulouse, CNRS, UPS, 205 route de Narbonne, BP44099, F-31077 Toulouse cedex 4, France; Email: laure.vendier@lcc-toulouse.fr

Iker del Rosal — LPCNO, CNRS & INSA, Université Paul Sabatier, 135 Avenue de Rangueil, 31077 Toulouse, France; Email: idel_ros@insa-toulouse.fr

Funding Sources

ERC Starting Grant (agreement 757501).

Notes

The authors declare no competing financial interest.

ACKNOWLEDGMENTS

D. S. and A. S. acknowledge the European Research Council (ERC) for funding (Grant Agreement 757501). A. C. is grateful to the French Ministry of National and Superior Education and Research (MENESR) for a Ph. D. fellowship. This work was performed using HPC resources from CALMIP (Grant 2017-[p17010]).

REFERENCES

(1) (a) *Transition Metal-Dinitrogen Complexes: Preparation and Reactivity*; Nishibayashi, Y., Ed.; Wiley-VCH Verlag GmbH & Co. KGaA: Weinheim, Germany, 2019. (b) *Nitrogen Fixation*;

Nishibayashi, Y., Ed.; Springer International Publishing AG: Cham, Switzerland, 2017. (c) Walter, M. D. Recent Advances in Transition Metal-Catalyzed Dinitrogen Activation. In *Advances in Organometallic Chemistry*; Pérez, P. J., Ed.; Academic Press, 2016; Vol. 65, pp 261–377. (d) Khoenkhoen, N.; de Bruin, B.; Reek, J. N. H.; Dzik, W. I. Reactivity of Dinitrogen Bound to Mid- and Late-Transition-Metal Centers. *Eur. J. Inorg. Chem.* **2015**, *2015*, 567–598. (e) MacKay, B. A.; Fryzuk, M. D. Dinitrogen Coordination Chemistry: On the Biomimetic Borderlands. *Chem. Rev.* **2004**, *104*, 385–402. (f) Gambarotta, S.; Scott, J. Multimetallic Cooperative Activation of N_2. *Angew. Chem. Int. Ed.* **2004**, *43*, 5298–5308. (g) Singh, D.; Buratto, W. R.; Torres, J. F.; Murray, L. J. Activation of Dinitrogen by Polynuclear Metal Complexes. *Chem. Rev.* **2020**, *120*, 5517–5581

(2) (a) Ertl, G. Reactions at Surfaces: From Atoms to Complexity (Nobel Lecture). *Angew. Chem. Int. Ed.* **2008**, *47*, 3524–3535. (b) Schlögl, R. Catalytic Synthesis of Ammonia—A "Never-Ending Story"? *Angew. Chem. Int. Ed.* **2003**, *42*, 2004–2008. (c) Smil, V. *Enriching the Earth: Fritz Haber, Carl Bosch, and the Transformation of World Food Production*; Mit Press, 2001. (d) Jennings, J. R. *Catalytic Ammonia Synthesis: Fundamentals and Practice*; Fundamental and Applied Catalysis; Springer, 1991.

(3) Hoffman, B. M.; Lukoyanov, D.; Yang, Z.-Y.; Dean, D. R.; Seefeldt, L. C. Mechanism of Nitrogen Fixation by Nitrogenase: The Next Stage. *Chem. Rev.* **2014**, *114*, 4041–4062.

(4) (a) Foster, S. L.; Bakovic, S. I. P.; Duda, R. D.; Maheshwari, S.; Milton, R. D.; Minteer, S. D.; Janik, M. J.; Renner, J. N.; Greenlee, L. F. Catalysts for Nitrogen Reduction to Ammonia. *Nat. Catal.* **2018**, *1*, 490–500. (b) Stucke, N.; Flöser, B. M.; Weyrich, T.; Tuczek, F. Nitrogen Fixation Catalyzed by Transition Metal Complexes: Recent Developments. *Eur. J. Inorg. Chem.* **2018**,

2018, 1337–1355. (c) Djurdjevic, I.; Einsle, O.; Decamps, L. Nitrogenase Cofactor: Inspiration for Model Chemistry. *Chem. Asian J.* **2017**, *12*, 1447–1455. (d) Roux, Y.; Duboc, C.; Gennari, M. Molecular Catalysts for N_2 Reduction: State of the Art, Mechanism, and Challenges. *ChemPhysChem* **2017**, *18*, 2606–2617. (e) Nishibayashi, Y. Recent Progress in Transition-Metal-Catalyzed Reduction of Molecular Dinitrogen under Ambient Reaction Conditions. *Inorg. Chem.* **2015**, *54*, 9234–9247. (f) Jia, H.-P.; Quadrelli, E. A. Mechanistic Aspects of Dinitrogen Cleavage and Hydrogenation to Produce Ammonia in Catalysis and Organometallic Chemistry: Relevance of Metal Hydride Bonds and Dihydrogen. *Chem. Soc. Rev.* **2014**, *43*, 547–564.

(5) Ashida, Y.; Arashiba, K.; Nakajima, K.; Nishibayashi, Y. Molybdenum-Catalysed Ammonia Production with Samarium Diiodide and Alcohols or Water. *Nature* **2019**, *568*, 536–540.

(6) Coffinet, A.; Simonneau, A.; Specklin, D. Push–Pull Activation of N_2: Coordination of Lewis Acids to Dinitrogen Complexes. In Encyclopedia of Inorganic and Bioinorganic Chemistry, R.A. Scott (Ed.) (2020). doi:10.1002/9781119951438.eibc2755

(7) (a) Chatt, J.; Dilworth, J. R.; Gunz, H. P.; Leigh, G. J.; Sanders, J. R. The Interaction of Dinitrogen Complexes of Rhenium and Osmium with Metal Salts. *J. Chem. Soc. D Chem. Commun.* **1970**, No. 2, 90–91. (b) Chatt, J.; Dilworth, J. R.; Leigh, G. J.; Richards, R. L. Polynuclear Dinitrogen Complexes. *J. Chem. Soc. D Chem. Commun.* **1970**, No. 15, 955–956. (c) Chatt, J.; Crabtree, R. H.; Richards, R. L. Dinitrogen- and Carbonyl-Complexes as Bases towards Trimethylaluminium. *J. Chem. Soc. Chem. Commun.* **1972**, No. 9, 534. (d) Chatt, J.; Crabtree, R. H.; Jeffery, E. A.; Richards, R. L. The Basic Strengths of Some Dinitrogen Complexes of Molybdenum(0), Tungsten(0), Rhenium(I), and Osmium(II). *J. Chem. Soc. Dalt. Trans.* **1973**, No. 11, 1167–1172.

(8) Sellman, D.; Gerlach, R.; Jödden, K. Reaktionen an Komplexgebundenen Liganden. XXXII.: Synthese Und Eigenschaften von Heteronuklearen Mangan-Chrom-Komplexen Mit Distickstoff-Diazen- Und Hydrazin-Brükenliganden. *J. Organomet. Chem.* **1979**, *178*, 433–447.

(9) (a) Mizobe, Y.; Yokobayashi, Y.; Oshita, H.; Takahashi, T.; Hidai, M. Preparation of Heterobimetallic Complexes with a Bridging Dinitrogen Ligand, $[WX(PMe_2Ph)_4(\mu\text{-}N_2)MCp_2Cl]$ (M = Ti, X = Cl; M = Zr, and Hf, X = I), and X-Ray Structure of $[WI(PMe_2Ph)_3(Py)(\mu\text{-}N_2)ZrCp_2Cl]$ (Py = Pyridine). *Organometallics* **1994**, *13*, 3764–3766. (b) Ishino, H.; Nagano, T.; Kuwata, S.; Yokobayashi, Y.; Ishii, Y.; Hidai, M.; Mizobe, Y. Syntheses, Structures, and Reactivities of Heterobimetallic Bridging Dinitrogen Complexes Containing Group 6 and Group 4 or 5 Transition Metals. *Organometallics* **2001**, *20*, 188–198. (c) Ishino, H.; Takemoto, S.; Hirata, K.; Kanaizuka, Y.; Hidai, M.; Nabika, M.; Seki, Y.; Miyatake, T.; Suzuki, N. Olefin Polymerization Catalyzed by Titanium–Tungsten Heterobimetallic Dinitrogen Complexes. *Organometallics* **2004**, *23*, 4544–4546.

(10) Seymore, S. B.; Brown, S. N. Kinetic Effects in Heterometallic Dinitrogen Cleavage. *Inorg. Chem.* **2006**, *45*, 9540–9550.

(11) (a) Silverthorn, W. E. Formation of a Cationic Binuclear Iron–Dinitrogen Compound from Molecular Nitrogen. *J. Chem. Soc. D Chem. Commun.* **1971**, No. 20, 1310–1311. (b) O'Donoghue, M. B.; Zanetti, N. C.; Davis, W. M.; Schrock, R. R. "Fixation" of Dinitrogen by Molybdenum and the Formation of a Trigonal Planar Iron-Tris[Molybdenum(Dinitrogen)] Complex. *J. Am. Chem. Soc.* **1997**, *119*, 2753–2754. (c) O'Donoghue, M. B.; Davis, W. M.; Schrock, R. R.; Reiff, W. M. Heterobimetallic Dinitrogen Complexes That Contain the $\{[N_3N]Mo\text{-}N{:}N\}$- Ligand. *Inorg. Chem.* **1999**, *38*, 243–252. (d) Zhang, Q.-F.; Chim, J. L. C.; Lai, W.; Wong, W.-T.; Leung, W.-H. Bridged

Dinitrogen Complexes of Iron and Chromium Porphyrins. *Inorg. Chem.* **2001**, *40*, 2470–2471. (e) Geri, J. B.; Shanahan, J. P.; Szymczak, N. K. Testing the Push–Pull Hypothesis: Lewis Acid Augmented N_2 Activation at Iron. *J. Am. Chem. Soc.* **2017**, *139*, 5952–5956.

(12) Simonneau, A.; Turrel, R.; Vendier, L.; Etienne, M. Group 6 Transition-Metal/Boron Frustrated Lewis Pair Templates Activate N_2 and Allow Its Facile Borylation and Silylation. *Angew. Chem. Int. Ed.* **2017**, *56*, 12268–12272.

(13) Simonneau, A.; Etienne, M. Enhanced Activation of Coordinated Dinitrogen with P-Block Lewis Acids. *Chem. Eur. J.* **2018**, *24*, 12458–12463.

(14) (a) Fürstner, A.; Davies, P. W. Catalytic Carbophilic Activation: Catalysis by Platinum and Gold Pi Acids. *Angew. Chem. Int. Ed.* **2007**, *46*, 3410–3449. (b) Gorin, D. J.; Toste, F. D. Relativistic Effects in Homogeneous Gold Catalysis. *Nature* **2007**, *446*, 395–403. (c) Hashmi, A. S. K. Gold-Catalyzed Organic Reactions. *Chem. Rev.* **2007**, *107*, 3180-3211. (d) Li, Z.; Brouwer, C.; He, C. Gold-Catalyzed Organic Transformations. *Chem. Rev.* **2008**, *108*, 3239–3265. (e) Jiménez-Núñez, E.; Echavarren, A. M. Gold-Catalyzed Cycloisomerizations of Enynes: A Mechanistic Perspective. *Chem. Rev.* **2008**, *108*, 3326–3350. (f) Arcadi, A. Alternative Synthetic Methods through New Developments in Catalysis by Gold. *Chem. Rev.* **2008**, *108*, 3266–3325. (g) *Gold Catalysis*; Toste, F. D., Michelet, V., Eds.; Imperial College Press: London, United Kingdom, 2014.

(15) Raubenheimer, H. G.; Schmidbaur, H. Gold Chemistry Guided by the Isolobality Concept. *Organometallics* **2011**, *31*, 2507–2522.

(16) Shanahan, J. P.; Szymczak, N. K. Hydrogen Bonding to a Dinitrogen Complex at Room Temperature: Impacts on N_2 Activation. *J. Am. Chem. Soc.* **2019**, *141*, 8550–8556.

(17) The only relevant example of gold-N_2 coordination found in the literature is the hydrazido compound $[(LAu)_6(N_2)]^{2+}$ with L = phopshine, formed from $[(LAu)_3(\mu\text{-}O)]^+$ and hydrazine: Shan, H.; Yang, Y.; James, A. J.; Sharp, P. R. Dinitrogen Bridged Gold Clusters. *Science* **1997**, *275*, 1460–1462.

(18) Stephan, D. W. The Broadening Reach of Frustrated Lewis Pair Chemistry. *Science* **2016**, *354*.

(19) (a) Campos, J. Dihydrogen and Acetylene Activation by a Gold(I)/Platinum(0) Transition Metal Only Frustrated Lewis Pair. *J. Am. Chem. Soc.* **2017**, *139*, 2944–2947. (b) Hidalgo, N.; Moreno, J. J.; Pérez-Jiménez, M.; Maya, C.; López-Serrano, J.; Campos, J. Evidence for Genuine Bimetallic Frustrated Lewis Pair Activation of Dihydrogen with Gold(I)/Platinum(0) Systems. *Chem. Eur. J.* **2020**, *26*, 5982–5993.

(20) Tang, C.; Liang, Q.; Jupp, A. R.; Johnstone, T. C.; Neu, R. C.; Song, D.; Grimme, S.; Stephan, D. W. 1,1-Hydroboration and a Borane Adduct of Diphenyldiazomethane: A Potential Prelude to FLP-N_2 Chemistry. *Angew. Chem. Int. Ed.* **2017**, *56*, 16588–16592.

(21) (a) Melen, R. L. A Step Closer to Metal-Free Dinitrogen Activation: A New Chapter in the Chemistry of Frustrated Lewis Pairs. *Angew. Chem. Int. Ed.* **2018**, *57*, 880–882. (b) Ruddy, A. J.; Ould, D. M. C.; Newman, P. D.; Melen, R. L. Push and Pull: The Potential Role of Boron in N_2 Activation. *Dalton Trans.* **2018**, *47*, 10377–10381.

(22) Gaussian09, revision D.01. Frisch, M. J.; Trucks, G. W.; Schlegel, H. B.; Scuseria, G. E.; Robb, M. A.; Cheeseman, J. R.; Scalmani, G.; Barone, V.; Mennucci, B.; Petersson, G. A.; Nakatsuji, H.; Caricato, M.; Li, X.; Hratchian, H. P.; Izmaylov, A. F.; Bloino, J.; Zheng, G.;

Sonnenberg, J. L.; Hada, M.; Ehara, M.; Toyota, K.; Fukuda, R.; Hasegawa, J.; Ishida, M.; Nakajima, T.; Honda, Y.; Kitao, O.; Nakai, H.; Vreven, T.; Montgomery, Jr., J. A.; Peralta, J. E.; Ogliaro, F.; Bearpark, M.; Heyd, J. J.; Brothers, E.; Kudin, K. N.; Staroverov, V. N.; Keith, T.; Kobayashi, R.; Normand, J.; Raghavachari, K.; Rendell, A.; Burant, J. C.; Iyengar, S. S.; Tomasi, J.; Cossi, M.; Rega, N.; Millam, J. M.; Klene, M.; Knox, J. E.; Cross, J. B.; Bakken, V.; Adamo, C.; Jaramillo, J.; Gomperts, R.; Stratmann, R. E.; Yazyev, O.; Austin, A. J.; Cammi, R.; Pomelli, C.; Ochterski, J. W.; Martin, R. L.; Morokuma, K.; Zakrzewski, V. G.; Voth, G. A.; Salvador, P.; Dannenberg, J. J.; Dapprich, S.; Daniels, A. D.; Farkas, O.; Foresman, J. B.; Ortiz, J. V.; Cioslowski, J.; Fox, D. J.; Gaussian, Inc., Wallingford CT, 2013.

(23) (a) Perdew, J. P.; Chevary, J. A.; Vosko, S. H.; Jackson, K. A.; Pederson, M. R.; Singh, D. J.; Fiolhais, C. Atoms, Molecules, Solids, and Surfaces: Applications of the Generalized Gradient Approximation for Exchange and Correlation. *Phys. Rev. B* **1992**, *46*, 6671–6687. (b) Becke, A. D. Density-functional Thermochemistry. III. The Role of Exact Exchange. *J. Chem. Phys.* **1993**, *98*, 5648–5652.

(24) Andrae, D.; Häußermann, U.; Dolg, M.; Stoll, H.; Preuß, H. Energy-Adjusted ab Initio Pseudopotentials for the Second and Third Row Transition Elements. *Theor. Chim. Acta* **1990**, *77*, 123–141.

(25) Ehlers, A. W.; Böhme, M.; Dapprich, S.; Gobbi, A.; Höllwarth, A.; Jonas, V.; Köhler, K. F.; Stegmann, R.; Veldkamp, A.; Frenking, G. A Set of F-Polarization Functions for Pseudo-Potential Basis Sets of the Transition Metals Sc□Cu, Y□Ag and La□Au. *Chem. Phys. Lett.* **1993**, *208*, 111–114.

(26) Grimme, S.; Ehrlich, S.; Goerigk, L. Effect of the Damping Function in Dispersion Corrected Density Functional Theory. *J. Comput. Chem.* **2011**, *32*, 1456–1465.

(27) (a) Reed, A. E.; Weinhold, F. Natural Bond Orbital Analysis of Near-Hartree–Fock Water Dimer. *J. Chem. Phys.* **1983**, *78*, 4066–4073. (b) Reed, A. E.; Curtiss, L. A.; Weinhold, F. Intermolecular Interactions from a Natural Bond Orbital, Donor-Acceptor Viewpoint. *Chem. Rev.* **1988**, *88*, 899–926.

(28) *trans*-$Mo(dppe)_2(N_2)_2$ and *trans*-$Mo(depe)_2(N_2)_2$ ($\mathbf{3}_{Mo}$) prepared from $MoCl_5$: (a) George, T. A.; Noble, M. E. A Direct One-Step Preparation of Bis(Dinitrogen) Complexes of Molybdenum(0) from Molybdenum(V) Chloride. *Inorg. Chem.* **1978**, *17*, 1678–1679. *trans*-$W(dppe)_2(N_2)_2$ ($\mathbf{2}_W$) prepared from $WCl_4(PPh_3)_2$: (b) Dilworth, J. R.; Richards, R. L. The Synthesis of Molybdenum and Tungsten Dinitrogen Complexes. *Inorg. Synth.* **1990**, *28*, 33–43. cis/trans mixture of $Mo(N_2)_2(PMe_2Ph)_4$ ($\mathbf{4}_{Mo}$) prepared from $MoCl_3(THF)_3$: (c) Anker, M. W.; Chatt, J.; Leigh, G. J.; Wedd, A. G. Preparation of Trichlorotris(Tetrahydrofuran)Molybdenum(III) and Its Use in the Preparation of Complexes of Molybdenum-(III) and -(0). *J. Chem. Soc. Dalt. Trans.* **1975**, No. 23, 2639–2645. *trans*-$W(depe)_2(N_2)_2$ ($\mathbf{3}_W$) and *cis*-$W(N_2)_2(PMe_2Ph)_4$ ($\mathbf{4}_W$) prepared from WCl_6: (d) Coffinet, A.; Specklin, D.; Vendier, L.; Etienne, M.; Simonneau, A. Frustrated Lewis Pair Chemistry Enables N_2 Borylation by Formal 1,3-Addition of a B–H Bond in the Coordination Sphere of Tungsten. *Chem. Eur. J.* **2019**, *25*, 14300–14303. *trans*-$W(depe)_2(^{15}N_2)_2$ prepared from *trans*-$[WCl_2(depe)_2]$ under an $^{15}N_2$ atmosphere: Filippou, A. C.; Schnakenburg, G.; Philippopoulos, A. I.; Weidemann, N. Ge_2 trapped via Triple Bonds between two Metal Centers: Syntheses and Structures of the Germylidyne Complexes *trans,trans* $[Cl(depe)_2M{\equiv}Ge{-}Ge{\equiv}M(depe)_2Cl]$ (M = Mo, W) and Bonding Analyses of the M≡Ge–Ge≡M chain. *Angew. Chem. Int. Ed.* **2005**, *44*, 5979–5985.

(29) Zheng, Y.; Zhang, J.; Cheng, X.; Xu, X.; Zhang, L. Wolff Rearrangement of Oxidatively Generated α-Oxo Gold Carbenes: An Effective Approach to Silylketenes. *Angew. Chem. Int. Ed.* **2019**, *58*, 5241–5245.

(30) Wang, C.; Erker, G.; Kehr, G.; Wedeking, K.; Fröhlich, R. Synthesis, Structural Features, and Formation of Organometallic Derivates of C1-Bridged Cp/Amido Titanium and Zirconium "CpCN-Constrained Geometry" Systems. *Organometallics* **2005**, *24*, 4760–4773.

(31) (a) Harris, R. K.; Becker, E. D.; Cabral de Menezes, S. M.; Granger, P.; Hoffman, R. E.; Zilm, K. W. Further Conventions for NMR Shielding and Chemical Shifts (IUPAC Recommendations 2008). *Pure Appl. Chem.* **2008**, *80*, 59–84. (b) Harris, R. K.; Becker, E. D.; Cabral de Menezes, S. M.; Goodfellow, R.; Granger, P. NMR Nomencalture. Nuclear Spin Properties and Conventions for Chemical Shifts. *Pure Appl. Chem.* **2001**, *73*, 1795–1818.

(32) (a) *N-Heterocyclic Carbenes: Effective Tools for Organometallic Synthesis*; Nolan, S. P., Ed.; Wiley-VCH Verlag GmbH & Co. KGaA: Weinheim, Germany, 2014. (b) Nolan, S. P. The Development and Catalytic Uses of N-Heterocyclic Carbene Gold Complexes. *Acc. Chem. Res.* **2011**, *44*, 91–100.

(33) (a) Baker, M. V; Barnard, P. J.; Brayshaw, S. K.; Hickey, J. L.; Skelton, B. W.; White, A. H. Synthetic, Structural and Spectroscopic Studies of (Pseudo)Halo(1,3-Di-Tert-Butylimidazol-2-Ylidine)Gold Complexes. *Dalton Trans.* **2005**, No. 1, 37–43. (b) Mézailles, N.; Ricard, L.; Gagosz, F. Phosphine Gold(I) Bis-(Trifluoromethanesulfonyl)Imidate Complexes as New Highly Efficient and Air-Stable Catalysts for the Cycloisomerization of Enynes. *Org. Lett.* **2005**, *7*, 4133–4136. (c) Kumar, M.; Jasinski, J.; Hammond, G. B.; Xu, B. Alkyne/Alkene/Allene-Induced Disproportionation of Cationic Gold(I) Catalyst. *Chem. Eur. J.* **2014**, *20*, 3113–3119.

(34) Tuczek, F.; Horn, K. H.; Lehnert, N. Vibrational Spectroscopic Properties of Molybdenum and Tungsten N2 and N2Hx Complexes with Depe Coligands: Comparison to Dppe Systems and Influence of H-Bridges. *Coord. Chem. Rev.* **2003**, *245*, 107–120 and references therein.

(35) Biasiolo, L.; Trinchillo, M.; Belanzoni, P.; Belpassi, L.; Busico, V.; Ciancaleoni, G.; D'Amora, A.; Macchioni, A.; Tarantelli, F.; Zuccaccia, D. Unexpected Anion Effect in the Alkoxylation of Alkynes Catalyzed by N-Heterocyclic Carbene (NHC) Cationic Gold Complexes. *Chem. Eur. J.* **2014**, *20*, 14594–14598.

(36) Hussain, W.; Leigh, G. J.; Ali, H. M.; Pickett, C. J.; Rankin, D. A. Dinitrogen Binding and Electrochemistry in Complexes of Molybdenum and Tungsten. *J. Chem. Soc. Dalt. Trans.* **1984**, 1703–1708.

(37) (a) Jia, M.; Bandini, M. Counterion Effects in Homogeneous Gold Catalysis. *ACS Catal.* **2015**, *5*, 1638–1652. (b) Ciancaleoni, G.; Belpassi, L.; Zuccaccia, D.; Tarantelli, F.; Belanzoni, P. Counterion Effect in the Reaction Mechanism of NHC Gold(I)-Catalyzed Alkoxylation of Alkynes: Computational Insight into Experiment. *ACS Catal.* **2015**, *5*, 803–814. (c) Lu, Z.; Han, J.; Okoromoba, O. E.; Shimizu, N.; Amii, H.; Tormena, C. F.; Hammond, G. B.; Xu, B. Predicting Counterion Effects Using a Gold Affinity Index and a Hydrogen Bonding Basicity Index. *Org. Lett.* **2017**, *19*, 5848–5851. (d) Schießl, J.; Schulmeister, J.; Doppiu, A.; Wörner, E.; Rudolph, M.; Karch, R.; Hashmi, A. S. K. An Industrial Perspective on Counter Anions in Gold Catalysis: On Alternative Counter Anions. *Adv. Synth. Catal.* **2018**, *360*, 3949–3959.

(38) Average W–P and W–Cl distances for $[W(Cl)_2(dppe)_2]$ = 2.50 Å and 2.42 Å: (a) Filippou, A. C.; Schnakenburg, G.; Philippopoulos, A. I. Trans-Di-chloro-bis-[Ethane-1,2-Diyl-bis-(Di-phenyl-phophine)-κ^2P,P′]-tungsten(II) Pentane Hemisolvate. *Acta Crystallogr. Sect.*

E **2003**, *59*, m602–m604. Average W-P and W-Cl distances for $[W(Cl)_2(dppe)_2][X]$ (X= BF_4^-, PF_6^-) = 2.54 Å and 2.32 Å: (b) Imaeda, M.; Nishihara, H.; Nakano, K.; Ichida, H.; Kobayashi, A.; Saito, T.; Sasaki, Y. Reactions of $[W(N_2)_2(Dpe)_2]$ with $HFeCo_3(CO)_{12}$ in Aqueous and Halogenated Solvents to Form Hydrazido(2-) Hydroxo Complexes of Tungsten(IV) and Dihalo Complexes of Tungsten(III). Crystal Structure of $[WCl_2(Dpe)_2]BF_4.1/3CH_2Cl_2$. *Inorg. Chem.* **1985**, *24*, 1246–1250. (c) Jayarathne, U.; Chandrasekaran, P.; Greene, A. F.; Mague, J. T.; DeBeer, S.; Lancaster, K. M.; Sproules, S.; Donahue, J. P. X-Ray Absorption Spectroscopy Systematics at the Tungsten L-Edge. *Inorg. Chem.* **2014**, *53*, 8230–8241.

(39) Gaillard, S.; Nun, P.; Slawin, A. M. Z.; Nolan, S. P. Expeditious Synthesis of Au(NHC)(L) (+) (NHC = N-Heterocyclic Carbene; L = Phosphine or NHC) Complexes. *Organometallics* **2010**, *29*, 5402–5408.

(40) (a) Azizian, H.; Luck, R.; H. Morris, R.; Wong, H. Dinitrogen versus H6-Arene Coordination in Methyldiphenylphosphine Complexes of Molybdenum(0). *J. Organomet. Chem.* **1982**, *238*, C24–C26. (b) Luck, R.; Morris, R. H. Reversible Binding of Dinitrogen and Dihydrogen by (η^6-Phenylmethylphenylphosphine)Tris(Methyldiphenylphosphine)Molybdenum (Mo(η^6-PhPMePh)(PMePh2)3): Use of [9-BBN]2 as a Phosphine Sponge Reagent. *Inorg. Chem.* **1984**, *23*, 1489–1491.

(41) The peculiar shape of the N_2 ligand in Figure is caused by a disorder of the two axial ligands within the crystal lattice.

(42) de Frémont, P.; Marion, N.; Nolan, S. P. Cationic NHC–Gold(I) Complexes: Synthesis, Isolation, and Catalytic Activity. *J. Organomet. Chem.* **2009**, *694*, 551–560.

(43) Gómez-Suárez, A.; Nelson, D. J.; Nolan, S. P. Quantifying and Understanding the Steric Properties of N-Heterocyclic Carbenes. *Chem. Commun.* **2017**, *53*, 2650–2660.

(44) Mean Mo–N double bonds = 1.752 Å (SD = 0.0485 Å) gathered from 760 structures of the SCD database. Mean W–N double bonds = 1.771 Å (SD = 0.0641 Å) gathered from 546 structures of the SCD database.

(45) Idipp* = 1,3-bis(2,6-bis(diphenylmethyl)-4-methylphenyl)imidazol-2-ylidene. Veenboer, R. M. P.; Gasperini, D.; Nahra, F.; Cordes, D. B.; Slawin, A. M. Z.; Cazin, C. S. J.; Nolan, S. P. Expedient Syntheses of Neutral and Cationic Au(I)–NHC Complexes. *Organometallics* **2017**, *36*, 3645–3653.

(46) Piascik, A. D.; Hill, P. J.; Crawford, A. D.; Doyle, L. R.; Green, J. C.; Ashley, A. E. Cationic Silyldiazenido Complexes of the Fe(Diphosphine)$_2$(N_2) Platform: Structural and Electronic Models for an Elusive First Intermediate in N_2 Fixation. *Chem. Commun.* **2017**, *53*, 7657–7660.

(47) Green, M. L. H.; Silverthorn, W. E. The μ-Dinitrogen-bis{[1,2-Bis(Dimethylphosphino)Ethane]Hydrido-[η-(1,3,5-Trimethylbenzene)]Molybdenum} Cation. *J. Chem. Soc. Dalt. Trans.* **1974**, No. 20, 2164–2166.

(48) Chatt, J.; Fay, R. C.; Richards, R. L. Preparation and Characterisation of the Dinuclear Dinitrogen Complex, Trichloro-μ-Dinitrogen-Bis(Tetrahydrofuran){chlorotetrakis[Dimethyl-(Phenyl)Phosphine]Rhenium(I)}chromium(III)[(PMe_2Ph)$_4$ClReN_2CrCl_3(Thf)$_2$]. *J. Chem. Soc. A Inorganic, Phys. Theor.* **1971**, No. 0, 702–704.

(49) Selected examples: (a) Welch, G. C.; Coffin, R.; Peet, J.; Bazan, G. C. Band Gap Control in Conjugated Oligomers via Lewis Acids. *J. Am. Chem. Soc.* **2009**, *131*, 10802–10803, B–N =

1.557 Å. (b) Herrmann, H.; Fillol, J. L.; Gehrmann, T.; Enders, M.; Wadepohl, H.; Gade, L. H. Bonding and Bending in Zirconium(IV) and Hafnium(IV) Hydrazides. *Chem. Eur. J.* **2008**, *14*, 8131–8146, B–N = 1.562 Å.

(50) Selected examples: (a) Welch, G. C.; Coffin, R.; Peet, J.; Bazan, G. C. Band Gap Control in Conjugated Oligomers via Lewis Acids. *J. Am. Chem. Soc.* **2009**, *131*, 10802–10803, B–N = 1.557 Å. (b) Herrmann, H.; Fillol, J. L.; Gehrmann, T.; Enders, M.; Wadepohl, H.; Gade, L. H. Bonding and Bending in Zirconium(IV) and Hafnium(IV) Hydrazides. *Chem. Eur. J.* **2008**, *14*, 8131–8146, B–N = 1.562 Å.

(51) Toyota, S.; Oki, M. Structure of Intramolecular Boron–Amine Complexes and Proposal of Tetrahedral Character for Correlation between Molecular Structure and Barrier to Dissociation of the N–B Bonds. *Bull. Chem. Soc. Jpn.* **1992**, *65*, 1832–1840.

(52) Donovan-Mtunzi, S.; Richards, R. L.; Mason, J. Nitrogen-15 Nuclear Magnetic Resonance Spectroscopy of Dinitrogen-bridged complexes. *J. Chem. Soc. Dalton Trans.* **1984**, 2429–2433.

(53) Dilworth, J. R. Diazene, Diazenido, Isodiazene and Hydrazido Complexes. *Coord. Chem. Rev.* **2017**, *330*, 53–94.

(54) (a) Comas-Vives, A.; Harvey, J. N. How Important Is Backbonding in Metal Complexes Containing N-Heterocyclic Carbenes? Structural and NBO Analysis. *Eur. J. Inorg. Chem.* **2011**, 5025–5035. (b) Marchione, D.; Belpassi, L.; Bistoni, G.; Macchioni, A.; Tarantelli, F.; Zuccaccia, F. The Chemical Bond in Gold(I) Complexes with N-Heterocyclic Carbenes. *Organometallics* **2014**, 33, 4200–4208. (c) Frenking, G.; Sola, M.; Vyboishchikov, S. F. Chemical bonding in transition metal carbene complexes. *J. Organomet. Chem.* **2005**, *690*, 6178–6204. (d) Nemcsok,

D.; Wichmann, K.; Frenking, G. The Significance of π Interactions in Group 11 Complexes with N-Heterocyclic Carbenes. *Organometallics* **2004**, *23*, 3640-3646

(55) Fontaine, P. P.; Yonke, B. L.; Zavalij, P. Y.; Sita, L. R. Dinitrogen Complexation and Extent of N≡N Activation within the Group 6 "End-On-Bridged" Dinuclear Complexes, {(η^5-C_5Me_5)M[N(*i*-Pr)C(Me)N(*i*-Pr)]}$_2$(μ-η^1:η^1-N_2) (M = Mo and W). *J. Am. Chem. Soc.* **2010**, *132*, 12273–12285.

(56) Jerabek, P.; Roesky, H. W.; Bertrand, G.; Frenking, G. Coinage Metals Binding as Main Group Elements: Structure and Bonding of the Carbene Complexes [TM(CAAC)$_2$] and [TM(CAAC)$_2$]$^+$ (TM = Cu, Ag, Au). *J. Am. Chem. Soc.* **2014**, *136*, 17123–17135.